doi:10.1093/plphys/kiaa051 PLANT PHYSIOLOGY 2021: 185: 405–423

Plant Physiology

Research Article

A temperature-sensitive *FERONIA* mutant allele that alters root hair growth

Daewon Kim [1,2], Jiyuan Yang [2], Fangwei Gu [2], Sungjin Park [2], Jonathon Combs [2], Alexander Adams,[3] Heather B. Mayes [3], Su Jeong Jeon,[1] Jeong Dong Bahk[1] and Erik Nielsen [2,*,†]

1 Division of Applied Life Sciences (BK21plus), Graduate School of Gyeongsang National University, Jinju 660-701, Republic of Korea
2 Department of Molecular, Cellular, and Developmental Biology, University of Michigan, Ann Arbor, Michigan 48109, USA
3 Department of Chemical Engineering, University of Michigan, Ann Arbor, Michigan 48109, USA

*Author for communication: nielsene@umich.edu
†Senior author.

E.N. conceived the original screening and research plans; J-D.B. and E.N. supervised the experiments; D.K., J.Y., F.G., S.P., SJ.J, and J.C. performed the in planta experiments and microscopy, and A.A. performed structural modeling and was supervised by H.B.M. D.K. wrote the article with contributions of all the authors; E.N. supervised and completed the writing, and agrees to serve as the author responsible for contact and ensures communication.
The author responsible for distribution of materials integral to the findings presented in this article in accordance with the policy described in the Instructions for Authors (https://academic.oup.com/plphys) is: Erik Nielsen (nielsene@umich.edu).

Abstract

In plants, root hairs undergo a highly polarized form of cell expansion called tip-growth, in which cell wall deposition is restricted to the root hair apex. In order to identify essential cellular components that might have been missed in earlier genetic screens, we identified conditional temperature-sensitive (ts) root hair mutants by ethyl methanesulfonate mutagenesis in *Arabidopsis thaliana*. Here, we describe one of these mutants, *feronia-temperature sensitive* (*fer-ts*). Mutant *fer-ts* seedlings were unaffected at normal temperatures (20°C), but failed to form root hairs at elevated temperatures (30°C). Map based-cloning and whole-genome sequencing revealed that *fer-ts* resulted from a G41S substitution in the extracellular domain of *FERONIA* (*FER*). A functional fluorescent fusion of FER containing the *fer-ts* mutation localized to plasma membranes, but was subject to enhanced protein turnover at elevated temperatures. While tip-growth was rapidly inhibited by addition of rapid alkalinization factor 1 (RALF1) peptides in both wild-type and *fer-ts* mutants at normal temperatures, root elongation of *fer-ts* seedlings was resistant to added RALF1 peptide at elevated temperatures. Additionally, at elevated temperatures *fer-ts* seedlings displayed altered reactive oxygen species (ROS) accumulation upon auxin treatment and phenocopied constitutive *fer* mutant responses to a variety of plant hormone treatments. Molecular modeling and sequence comparison with other *Catharanthus roseus* receptor-like kinase 1L (CrRLK1L) receptor family members revealed that the mutated glycine in *fer-ts* is highly conserved, but is not located within the recently characterized RALF23 and LORELI-LIKE-GLYCOPROTEIN 2 binding domains, perhaps suggesting that *fer-ts* phenotypes may not be directly due to loss of binding to RALF1 peptides.

Introduction

In land plants, root hairs are cellular protuberances resulting from the polarized outgrowth of specialized root epidermal cells, known as trichoblasts (Gilroy and Jones, 2000). Root hair development can be divided into three phases: cell specification, initiation of bulge formation, and polarized tip growth (Cho and Cosgrove, 2002). Polarized tip growth results from the integration of highly specific exocytosis of Golgi-derived vesicles containing newly synthesized cell

Received October 29, 2020. Accepted November 14, 2020. Advance access publication December 7, 2020

wall material at a restricted area of the root hair tip, with a tip-focused cytoplasmic calcium (Ca^{2+}) gradient ensuring correct targeting of this polarized membrane trafficking (Hepler et al., 2001; Smith et al., 2005; Cole and Fowler, 2006). This Ca^{2+} gradient is established by localized generation of reactive oxygen species (ROS) by *ROOT HAIR DEFECTIVE2* (*RHD2*), which encodes an NADPH oxidase in *Arabidopsis thaliana* (Foreman et al., 2003). RHO OF PLANTS (ROP) small GTPase-mediated signal transduction is involved in specifying the root hair initiation site and future root hair elongation by stimulating *RHD2* activity at the growing root hair apex (Molendijk et al., 2001; Jones et al., 2002; Carol and Dolan, 2006). Recently, a number of receptor-like kinases (RLKs) have been identified that are involved in cellular growth regulation, including the cell elongation associated with root hair tip growth (Shiu and Bleecker, 2001; Lehti-Shiu et al., 2009; Lindner et al., 2012). In particular, CrRLK1L subfamily proteins, which includes *FERONIA* (*FER*; Huck et al., 2003), *ERELUS* (*ERE*; Haruta et al., 2014; Schoenaers et al., 2018), *THESEUS1* (*THE1*; Hematy et al., 2007), and *ANXUR1/2* (Miyazaki et al., 2009), have been implicated in cell wall sensing associated with a variety of cellular events such as female fertility, cell elongation, root-hair development, mechano-sensing, and responses to hormones and pathogens (Boisson-Dernier et al., 2009; Cheung and Wu, 2011; Lindner et al., 2012).

The CrRLK1L subfamily is named after the first member functionally characterized in *Catharanthus roseus* cell cultures (Schulze-Muth et al., 1996), and Arabidopsis contains 17 CrRLK1L subfamily members (Hematy and Hofte, 2008). The majority of CrRLK1L RLK proteins are predicted serine/threonine kinases with a single transmembrane domain between an N-terminal extracellular domain containing two tandem domains with limited homology to the carbohydrate-binding domain of animal malectin proteins, and a C-terminal cytoplasmic kinase domain (Schallus et al., 2008; Cheung and Wu, 2011). *THE1* was discovered in a screen for suppressors that partially restored the dark-grown hypocotyl growth defect of *procuste1-1 (prc1-1)*, which is defective in the cellulose synthase catalytic subunit CESA6 (Hematy et al., 2007). *HERCULES1* (*HERK1*), was identified as functionally redundant with *THE1* in modulating cell elongation (Guo et al., 2009). While single mutant *the1* or *herk1* plants displayed normal growth, *the1 herk1* double mutants were severely stunted (Guo et al., 2009). *ANXUR1* and *ANXUR2* (*ANX1* and *ANX2*) are exclusively expressed in the male gametophyte (Boisson-Dernier et al., 2009) and function in maintaining pollen tube wall integrity during migration through floral tissues until their deactivation allows the pollen to burst during fertilization (Boisson-Dernier et al., 2009).

Similar to *ANX1* and *ANX2*, *FER*, which is allelic to *SIRÈNE (SRN)*, was initially identified in the regulation of female control of fertility (Huck et al., 2003), and is highly expressed in the synergid cells of the female gametophyte and in a variety of vegetative tissues, but not in the male gametophyte (Escobar-Restrepo et al., 2007; Guo et al., 2009). In the female gametophyte, *FER* is involved in sensing pollen tube arrival and promoting its rupture (Huck et al., 2003; Rotman et al., 2003), and in the initiation of programmed cell death of one of two synergid cells during the double fertilization event (Ngo et al., 2014). *FER* also inhibits polyspermy through regulation of demethylesterified pectin accumulation in the filiform apparatus of the ovule (Duan et al., 2020).

In addition to its important roles during fertilization, *FER* has also been shown to regulate aspects of root hair elongation (Duan et al., 2010; Huang et al., 2013), calcium signaling during mechanical stimulation of roots (Shih et al., 2014), and cell wall responses to both abiotic and biotic stress (Huck et al., 2003; Rotman et al., 2003; Lindner et al., 2012; Duan et al., 2014; Ngo et al., 2014; Shih et al., 2014; Li et al., 2016). *FER* was shown to bind to a ROP guanidine exchange factor 1 (ROPGEF1) that activates ROP GTPase signaling during root hair tip-growth in Arabidopsis (Duan et al., 2010). *FER*, and other members of the CrRLK1L receptor family, have been proposed to bind to secreted rapid alkalinization factor (RALF) peptide ligands (Haruta et al., 2014), with RALF1 binding the *FER* extracellular domain to suppress cell elongation of the primary root (Haruta et al., 2014). RALF34 binds to *THE1* during regulation of lateral root initiation (Gonneau et al., 2018), and RALF23 binding to *FER* negatively regulates plant immune responses (Stegmann et al., 2017). *FER* was shown to associate with a glycosylphosphatidylinositol-anchored co-receptor, *LORELEI* (*LRE*; Liu et al., 2016), and a crystal structure of the FER extracellular domain bound to a LRE-like protein (LLG2), and RALF23 shows that LLG2 and RALF23 peptides associate with the second malectin-like domain (Xiao et al., 2019).

Although RALF peptide binding occurs in several CrRLK1L RLKs, it remains unclear whether this is the only ligand recognized by this class of RLKs. Indeed, *the1-1* mutants displayed altered growth phenotypes despite the *the1-1* mutant extracellular domain being able to bind RALF34 (Gonneau et al., 2018). Additionally, while RALF peptides appear to only bind the second of two malectin-like domains in the FER extracellular domain, both these domains appear to associate with pectin polysaccharides (Feng et al., 2018). We have identified a new temperature-sensitive mutation (*fer-ts*) in a highly conserved glycine residue (G41S) present in the extracellular domain of the FER receptor kinase, as well as other members of the CrRLK1L RLK family and mammalian malectin sequences. The *fer-ts* mutant exhibited rapid cessation of root hair tip-growth within 1 min upon transferal to elevated (30°C) growth temperatures. This rapid cessation of root hair tip growth was also observed when *fer-4* null mutants were transformed with a fluorescently tagged version of the temperature-sensitive FER(G41S)-EYFP fusion protein. FER(G41S)-EYFP was still present in the plasma membrane in root hairs that had ceased tip-growth, indicating that the primary defect of this mutant is due to failure to properly transmit extracellular signals at elevated temperatures. These findings provide a powerful

new tool for dissecting how FERONIA, and potentially other CrRLK1L RLKs, function during plant growth and development.

Results

Isolation of a temperature-sensitive mutant that inhibits root hair tip growth

The regulatory GTPase, RabA4b, participates in membrane trafficking associated with the polarized secretion of cell wall components in plant cells. In addition, loss of tip localization of EYFP-RabA4b is highly correlated with inhibition of root hair tip growth (Preuss et al., 2004). In order to identify additional, potentially essential, molecular components that control root hair tip growth, ethyl methanesulfonate (EMS)-mutagenized seeds of a stable transgenic Arabidopsis line expressing EYFP-RabA4b were screened for seedlings with wild-type (WT) root hairs at normal temperatures (20°C), but which displayed impaired root hair growth when grown at elevated temperatures (30°C). The progeny of approximately 6,000 EMS-mutagenized seeds were screened. From the screening, four temperature-sensitive (ts-) root hair growth defect mutants were isolated, which we initially termed Loss-of-Tip-Localization mutants (*ltl1* to *ltl4*). Among these *ltl ts* mutants, *ltl2*, (subsequently referred to as *fer-ts*) root hair growth characteristics were examined under normal and elevated temperature conditions. In normal growth conditions (20°C), *fer-ts* root hairs displayed normal growth. However, both root hair growth and apical accumulation of EYFP-RabA4b of *fer-ts* root hairs were dramatically inhibited at 30°C (Figure 1A and B).

To quantify root hair elongation in *fer-ts* seedlings under normal and elevated temperature conditions, both root hair lengths and root hair density were measured. No significant differences were found between WT and *fer-ts* seedlings either in mature root hair length or in the number of root hairs per unit root length when plants were grown at 20°C. However, both length of root hairs and root hair density were greatly reduced in *fer-ts* plants grown at 30°C (Figure 1C and D). Primary root length and root growth rates of *fer-ts* seedlings were indistinguishable from WT at 20°C, but while WT roots grew slightly faster at 30°C, *fer-ts* primary root growth rates remained unchanged at elevated temperatures (Supplemental Figure S1). These results indicated that, at least in early stages of seedling growth and development, *fer-ts* temperature-sensitive defects are largely specific to root hair elongation in elevated temperature conditions.

In order to characterize the effects of the *fer-ts* mutation on root hair growth dynamics, elongating root hairs were visualized by time-lapse microscopy for 2 h. Seven-day-old *fer-ts* seedlings were placed in a temperature-controlled plant growth chamber at 20°C for 50 min and then the temperature of the chamber was rapidly transitioned to 30°C (Figure 2; dashed line). While root hair growth was unaffected by temperature transition in WT plants, transition to elevated temperatures resulted in rapid cessation of tip-growth in the *fer-ts* mutant (Figure 2 and Supplemental Movie S1).

Since root hair growth is tightly linked to accumulation of EYFP-RabA4b compartments in root hair tips (Preuss et al., 2004, 2006; Thole et al., 2008), we were interested in how this localization was affected upon transition from 20°C to 30°C in the *fer-ts* mutants. EYFP-RabA4b labeled compartments were maintained in the apical region of growing *fer-ts* root hairs at 20°C, but tip localization of these EYFP-RabA4b labeled membranes was rapidly lost upon transition to 30°C (Figure 3). EYFP-RabA4b accumulation was examined in WT and *fer-ts* plants in a temperature-controlled chamber at 20°C for 14 min, and then the chamber was rapidly transitioned to 30°C (Figure 3A; Supplemental Figure S2). Images of growing root hairs were collected at 1-min intervals by time-lapse confocal microscopy, and tip-localized EYFP signal was quantified in both WT (Figure 3B) and *fer-ts* root hairs (Figure 3C) root hairs. While tip-localized EYFP-RabA4b signal was unaffected by transition from 20°C to 30°C in WT root hairs (Figure 3B; triangles), tip-localized EYFP-RabA4b was significantly reduced in *fer-ts* root hairs within 1 min of the transition from 20°C to 30°C (Figure 3C; triangles).

Map-based cloning and full-genome sequencing identified the *fer-ts* locus

To identify the mutant locus responsible for the rapid, temperature-sensitive loss of root hair elongation and tip-localization of EYFP-RabA4b labeled compartments, a combination of map-based cloning and full-genome sequencing of *fer-ts* plants was performed. F_2 mapping populations were obtained by reciprocal crosses of back-crossed mutants (Col-0) with L*er* WT plants (Bell and Ecker, 1994), and segregating F_2 populations were used for subsequent map-based cloning. The temperature-sensitive mutant lesion was mapped to chromosome 3 between the simple sequence length polymorphism (SSLP) markers *NIT1.2* and *NGA6*, and subsequently to ~2 Mb region between *NIT1.2* and *CIW19* (Figure 4A). Whole-genome sequencing identified that the *fer-ts* mutant locus within this ~2 Mb region was due to a G121A nucleotide replacement resulting in a G41S substitution mutation within the extracellular domain of the previously characterized FER RLK (Figure 4B and C). In order to eliminate the possibility that this G→A substitution influenced the accumulation of *FER* mRNA at the transcriptional level, we performed reverse transcription–PCR (RT-PCR) analysis. *FERONIA* transcript levels of the *fer-ts* mutant were unchanged from those in WT plants (Figure 4D).

The G41S mutation in *fer-ts* is in a highly conserved glycine residue in CrRLK1L subfamily proteins

The G41S substitution of the *fer-ts* mutant rapidly inactivated *FER* function during root hair growth at elevated temperatures. In addition, a similar G37D mutation is responsible for inactivation of THE1, another member of the CrRLK1L family (Hematy et al., 2007), and multiple sequence

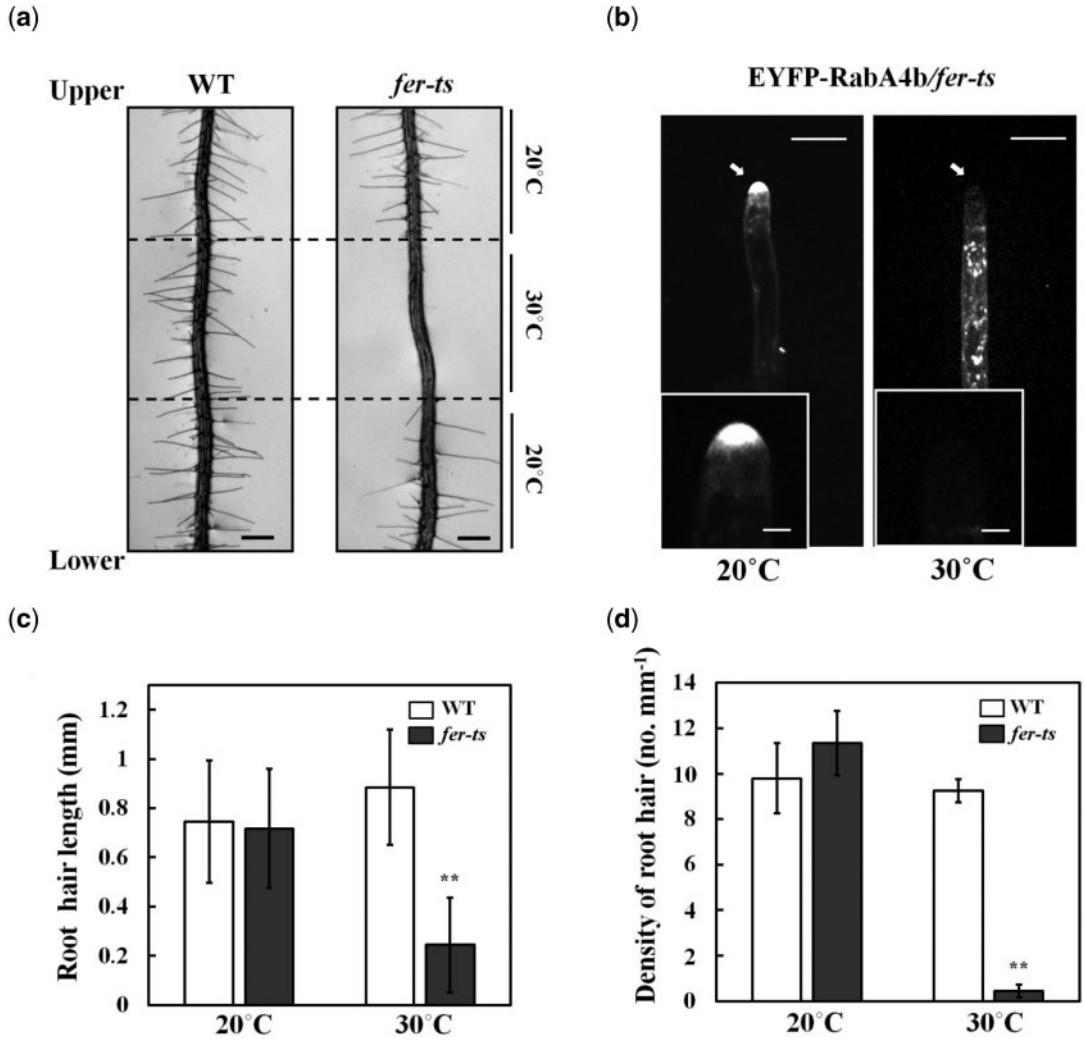

Figure 1 Isolation of a temperature-sensitive root hair growth defect mutant. (**A**), Seven day-old seedlings were grown vertically in 1/4 MS media under 20°C and transferred to 30°C for 6 h, followed by 24 h recovery at 20°C. Bright field images were collected with a Nikon Eclipse E600 wide-field microscope with a 10× Plan Apo DIC (0.75 NA) lens. Dashed lines indicate root tip positions when seedling plants were transferred to 30°C for 6 h, and again when they were transferred back to 20°C. Scale bars = 200 μm. B, Localization of EYFP-RabA4b protein in growing root hair cells of *fer-ts* mutants at 20°C and 30°C. Medial root hair sections were collected using spinning-disk confocal microscopy from growing root hair cells of 7-d-old seedlings stably expressing EYFP-RabA4b in the *fer-ts* mutant in 20°C (left) or 30°C (right) using a Zeiss 40× Plan-Apochromat (1.3 NA) lens and appropriate EYFP fluorescence filter sets. Scale bars = 10 μm. Insets, magnified images to show details of EYFP-RabA4b subcellular localization in root hair tips. Scale bars = 2 μm. C, Quantification of root hair length in WT and *fer-ts* mutants under 20°C [WT {n = 392}, *fer-ts* {n = 454}] and 30°C [WT {n = 185}, *fer-ts* {n = 23}] conditions. D, Calculation of root hair densities in WT and *fer-ts* mutants at 20°C [WT {n = 392}, *fer-ts* {n = 454}] and 30°C [WT {n = 185}, *fer-ts* {n = 23}] in fully expanded primary roots of 7-d old plants. In each case, root hair lengths and densities were measured from n = 20 individual seedlings. Error bars represent SD. $^{**}P < 0.001$ by Student's t test.

alignment analysis with other Arabidopsis CrRLK1L family members as well as animal malectin sequences showed that the G41 residue of FERONIA is absolutely conserved in these malectins and malectin-like 1 (ML1) domains (Figure 5A; Supplemental Figure S3). Interestingly, based on structural studies of animal malectin proteins, five key residues (Y67, Y89, Y116, F117, D186; Figure 5B, red residues) were found to form contacts with a bound disaccharide ligand, nigerose, in the active site as determined by structural analysis of the *Xenopus laevis* malectin protein (Schallus et al., 2008; Muller et al., 2010). In this malectin structure, these surface exposed residues extend from the malectin fold forming the nigerose-binding pocket, with the conserved glycine (G40) at the bottom of this structural region (Figure 5B). While several of the tyrosine and phenylalanine residues shown to be important for interaction with carbohydrates in animal malectin proteins are maintained in plant malectin-like domains (e.g. FERONIA Y88, Y114, F115, D197; Figure 5A; Supplemental Figure S3), these are not surface exposed in the ML1 domain of the recently described FER crystal structure (Figure 5C, in green) with its co-receptor LLG2 (Figure 5C, in blue) and a RALF23 ligand (Figure 5C, in magenta; Xiao et al., 2019). It is, however, notable that in this structure the invariant glycine (G41; Figure 5C, red residue)

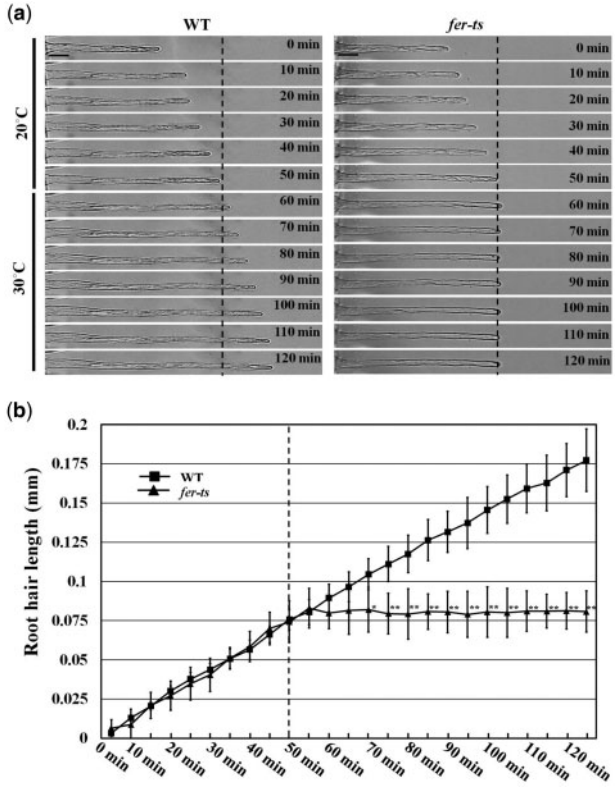

Figure 2 Root hair growth dynamics in WT and *fer-ts* seedlings. (**A**) Root hair tip-growth in WT and *fer-ts* mutant plants under normal (20°C) and elevated (30°C) temperatures by time-lapse microscopy. Bright field images of growing root hairs of WT and *fer-ts* mutant plants were collected every minute by time-lapse microscopy using a Zeiss 40× Plan-Apochromat (1.3 NA) lens. Representative images of WT and *fer-ts* mutant root hair elongation are presented at 10-min intervals. Scale bars = 10 μm. (**B**) Quantitative analysis of WT (n = 4) and *fer-ts* mutant (n = 4) root hair lengths upon transition to 30°C. WT (black squares) and *fer-ts* (black triangles) mutant root hair elongation were measured every 5 min and root hair lengths were determined using the measure function in Image J. The dashed line indicates the transition from 20°C to 30°C. Error bars represent SD. $^{*}P < 0.05$, $^{**}P < 0.01$ by Student's t test.

of the FER ML1 domain is not located within or nearby the RALF23 and LLG2 binding surfaces in the ML2 domain (Xiao et al., 2019).

The *fer-ts* phenotypes were confirmed by reciprocal crossing with FERONIA mutants and complementation assays

To confirm that the temperature-sensitive root hair defects and loss of tip-localized EYFP-RabA4b were causally linked to the G41S mutation in the FER locus, *fer-ts* mutant plants were reciprocally crossed with two previously characterized *FER* mutants, *fer-4* and *fer-5* (Duan et al., 2010). While both *fer-4* and *fer-5* fail to accumulate WT root hairs, *fer-4* produced no FER protein, while *fer-5* was shown to accumulate a truncated FER protein missing a functional cytosolic protein kinase domain (Duan et al., 2010). As a control, F1 plants of *fer-ts* crossed to WT plants displayed normal root hair growth in both normal and elevated temperature conditions, confirming that the *fer-ts* mutation is recessive (Figure 6A). However, F1 plants of either *fer-ts* (paternal line) crossed with *fer-4* and *fer-5* mutants (maternal lines; Figure 6A), or *fer-ts* (maternal line) crossed with *fer-4* and *fer-5* mutants (paternal line; Supplemental Figure S4a) displayed root hairless ts-phenotypes at elevated temperatures, respectively. These F1 plants were confirmed by genomic DNA PCR analysis with primers that discriminated between the *fer-ts* (or WT) *FER* loci and *fer-4* and *fer-5* T-DNA insertion mutant loci (Figure 6B and C, and Supplemental Figure S4b).

To verify that the FER G41S mutation specifically conferred the temperature-sensitive root hair phenotype, a fluorescently tagged FER-EYFP containing the G41S mutation, FER(G41S), driven by endogenous *FER* promoter sequences, was transformed into *fer-4* and *fer-5* mutant plants. Transgenic *fer-4* and *fer-5* plants expressing mutant FER(G41S)-EYFP proteins showed rescued root hair growth defects in these two *fer* mutant backgrounds in a temperature-sensitive manner (Figure 6D). Finally, a WT fluorescently tagged FER-EYFP, driven by endogenous *FER* promoter sequences (FER(WT)-EYFP), was able to fully rescue *fer-ts* root hair defects. FER(WT)-EYFP protein was detected in plasma membranes and *fer-ts* transgenic lines stably transformed, and homozygous for FER(WT)-EYFP displayed the normal root hair growth at both 20°C and 30°C (Figure 6E). As observed previously (Duan et al., 2010), pFER-FER(WT)-EYFP fluorescent fusions localized primarily to plasma membranes in both root cortical and mature root hair cells in these transgenic lines, although a small amount of pFER-FER(WT)-EYFP could also be seen in subcellular compartments that colocalized with FM 4-64 (Figure 6F). Taken together, these data strongly support that the *fer-ts* phenotype is the result of the G41S mutation of the FERONIA protein.

FERONIA is primarily localized to the plasma membranes and the *fer-ts* G41S substitution does not alter its subcellular localization

Previously, GFP-fused FERONIA was shown to localize to plasma membranes in various plant tissues (Duan et al., 2010). At normal temperatures, FER(WT)-EYFP was observed primarily in plasma membranes in various tissues such as leaf, root, and in mature root hairs (Figures 6F and 7A). At higher magnification, FER(WT)-EYFP was restricted to plasma membranes, and did not display significant accumulation in intracellular compartments in nontip-growing root cortical cells (Figure 7B). Interestingly, in actively growing root hairs, FER(WT)-EYFP protein was observed both in plasma membranes and an apical localized vesicle population (Supplemental Movie S2). To determine whether the introduction of the G41S substitution in the *fer-ts* mutant might affect the subcellular localization of this protein in normal or elevated temperatures, we compared the subcellular distributions of FER(WT)-EYFP and FER(G41S)-EYFP at

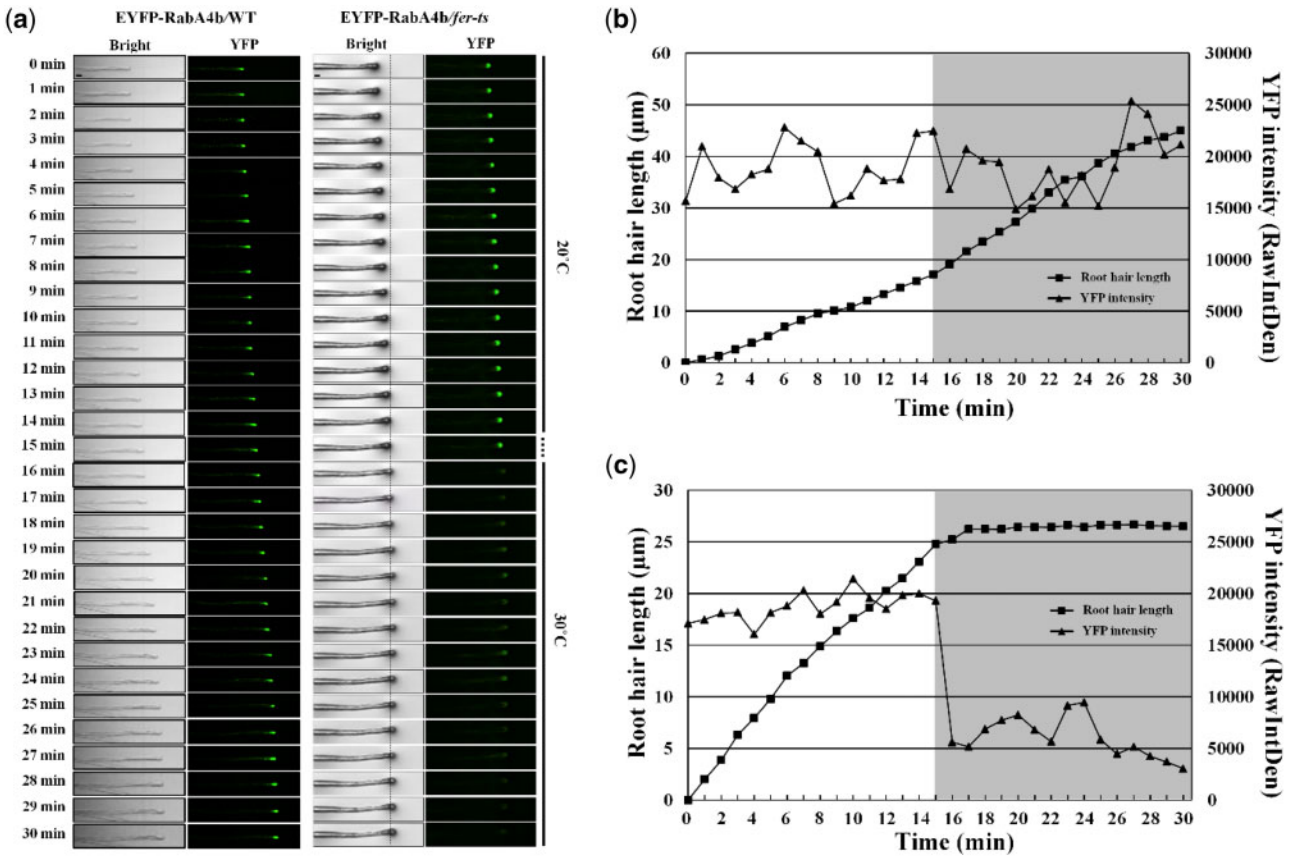

Figure 3 Temperature-sensitive subcellular dynamics of EYFP-RabA4b labeled compartments in growing root hairs in *fer-ts* mutants. (**A**) Localization of EYFP-RabA4b protein in growing root hair cells of WT and *fer-ts* mutant plants at normal (20°C) or elevated (30°C) temperature conditions. Growing WT and *fer-ts* root hairs were imaged at 1-min intervals for 30 min at 20°C at which the growth chamber temperature was raised to 30°C. For each time point, both bright field (Bright) and fluorescence (YFP) images were collected sequentially, and tip-localized EYFP-RabA4b compartments were monitored by spinning-disk fluorescence confocal microscopy using a Zeiss 40× Plan-Apochromat (1.3 NA) lens with appropriate EYFP fluorescence filter sets. The vertical line indicates when the temperature was raised to 30°C. Scale bars = 10 μm. Quantification of root hair elongation and EYFP-RabA4b root hair tip localization in WT (**B**) and *fer-ts* mutant (**C**) plants. Root hair length and EYFP-RabA4b fluorescence were quantified by Image J every 1 min. The gray box indicates when the temperature was raised to 30°C.

both 20°C and 30°C (Figure 7C and D). While no changes in accumulation or distribution of FER(WT)-EYFP were observed in roots and mature root hairs between 20°C and 30°C conditions (Figure 7C), at 30°C some FER(G41S)-EYFP fluorescence could be observed in internal subcellular membranes, although substantial levels of the FER(G41S)-EYFP remained at the plasma membranes in these cells even after extended incubation at 30°C for 6 h (Figure 7D).

Since the *fer-ts* mutant showed rapidly inhibited tip-growth upon transition to elevated temperatures (30°C), we were interested to determine how this might affect FER(G41S)-EYFP localization in actively growing root hair cells. Seven-day-old *fer-ts* seedlings were placed in a temperature-controlled plant growth chamber at 20°C and images of growing root hairs of plants stably expressing FER(WT)-EYFP or FER(G41S)-EYFP were collected every 5 s for at least 5 min, and then the temperature of the chamber was rapidly transitioned to 30°C (Figure 8A) to observe the effects of elevated temperatures on both root hair elongation as well as subcellular dynamics of FER(WT)-EYFP and FER(G41S)-EYFP proteins. As noted previously, EYFP(WT)-EYFP as well as FER(G41S)-EYFP localized to both plasma membranes and apically localized vesicle populations in growing root hairs at 20°C (Figure 8A; Supplemental Movie S3). However, while root hair growth and FER(WT)-EYFP localization were unaffected by elevated temperature (30°C), both tip-growth and accumulation of apically localized vesicles were inhibited within 1 min of transition to elevated temperature (Figure 8, C and D; Supplemental Movie S3). While FER(G41S)-EYFP in apically localized vesicles was rapidly lost upon cessation of tip-growth, plasma membrane localized FER(G41S)-EYFP levels did not decline with similar kinetics. Interestingly, after several minutes of elevated temperature the ratio of FER(G41S)-EYFP localized in an apical plasma membrane domain (Figure 8B, red) versus in flanking plasma membrane regions (Figure 8B, blue) declined (Figure 8E), perhaps reflecting either inhibition of secretion to the apical plasma membrane domain, or possibly due to destabilization of the FER(G41S)-EYFP protein at elevated temperatures.

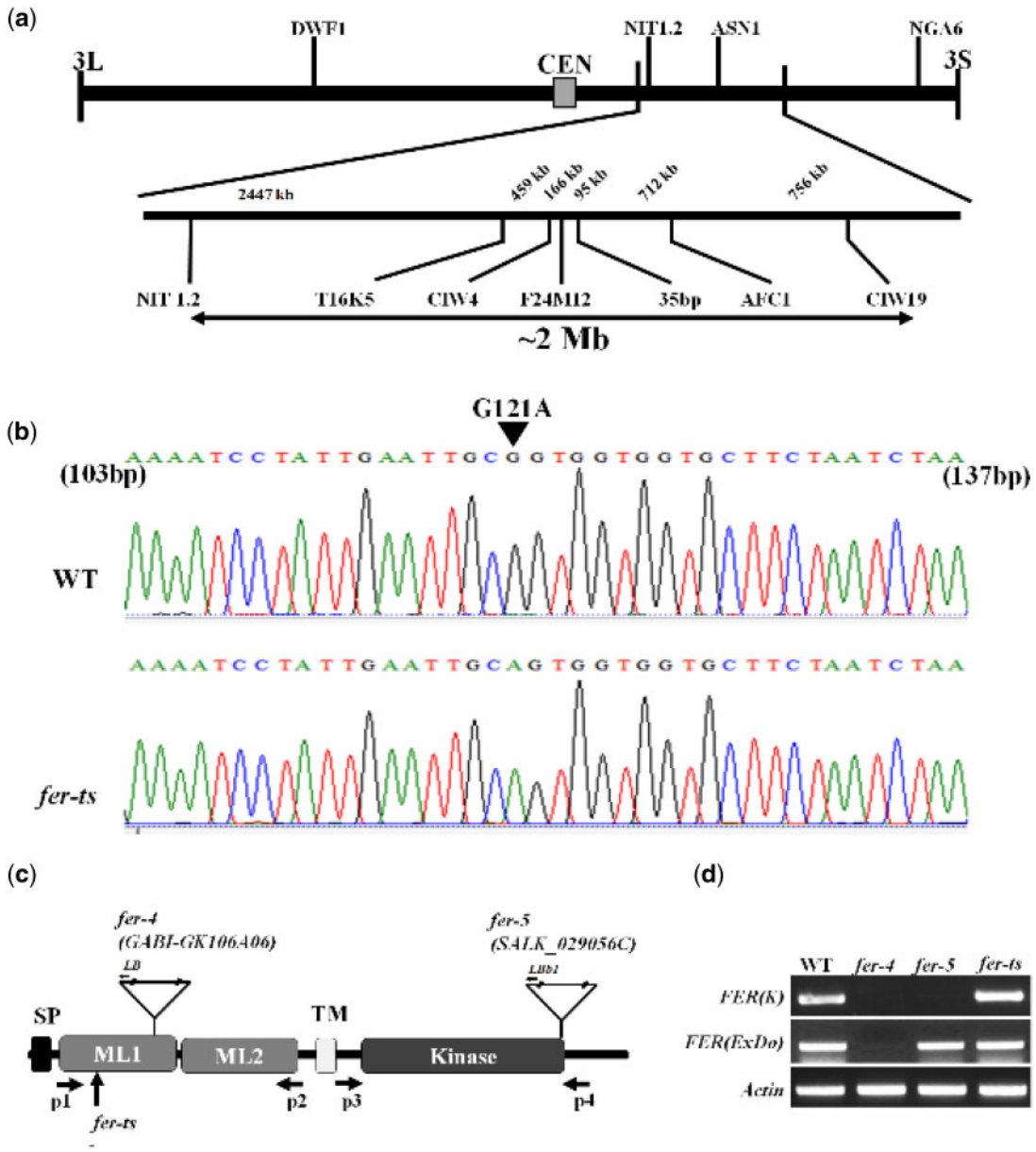

Figure 4 Map-based cloning of *fer-ts*. (**A**) A linear diagram of the Arabidopsis third chromosome is shown, with a magnified F24M12 marker region displayed below. The centromere is indicated with a filled-rectangle. Low-resolution map-based cloning resulted in identification of the *fer-ts* locus within ~2 Mb region of chromosome III bounded by markers NIT1.2 and CIW19. (**B**) SNPs specific to the ts-mutant within this region were identified using whole genomic resequencing, followed by targeted resequencing of genomic DNA of *fer-ts* and WT parental lines. A single G→A substitution was found in *FERONIA* (At3g51550). The arrowhead indicates the G121A substituted mutation in the *FERONIA* gene locus. (**C**) Schematic diagram of FERONIA protein domains and mutation regions, composed of an N-terminal extracellular domain (tandem repeat malectin-like domains; ML1 and ML2), TM (transmembrane) domain in the middle region and a C-terminal kinase domain (serine/threonine kinase), the end of the N-terminus has a signal peptide (SP) sequence for plasma-membrane trafficking. The *fer-4* and *fer-5* mutants displayed that T-DNA was inserted in malectin-like domain 1 and kinase domain, respectively. (**D**) RT-PCR analysis of the T-DNA inserted mutants and EMS mutants. The FER(ExDo) and FER(K) domains were amplified using P1 and P2 primers and P3 and P4 primers, respectively, Actin was used as a loading control.

In order to examine whether the *fer-ts* mutant protein might display increased protein turnover we blocked new protein synthesis by treating 5-d-old Arabidopsis seedlings with cycloheximide, and then compared protein turnover rates of the FER(WT)-EYFP and FER(G41S)-EYFP proteins when grown at 30°C. Overall, accumulation of the FER(G41S)-EYFP was reduced significantly during the time course, but no significant reduction in protein accumulation was observed for either EYFP(WT)-EYFP or an actin loading control (Figure 8F). These results suggest that while rapid cessation of tip-growth in root hairs occurs within one minute of transition to elevated temperatures, that upon

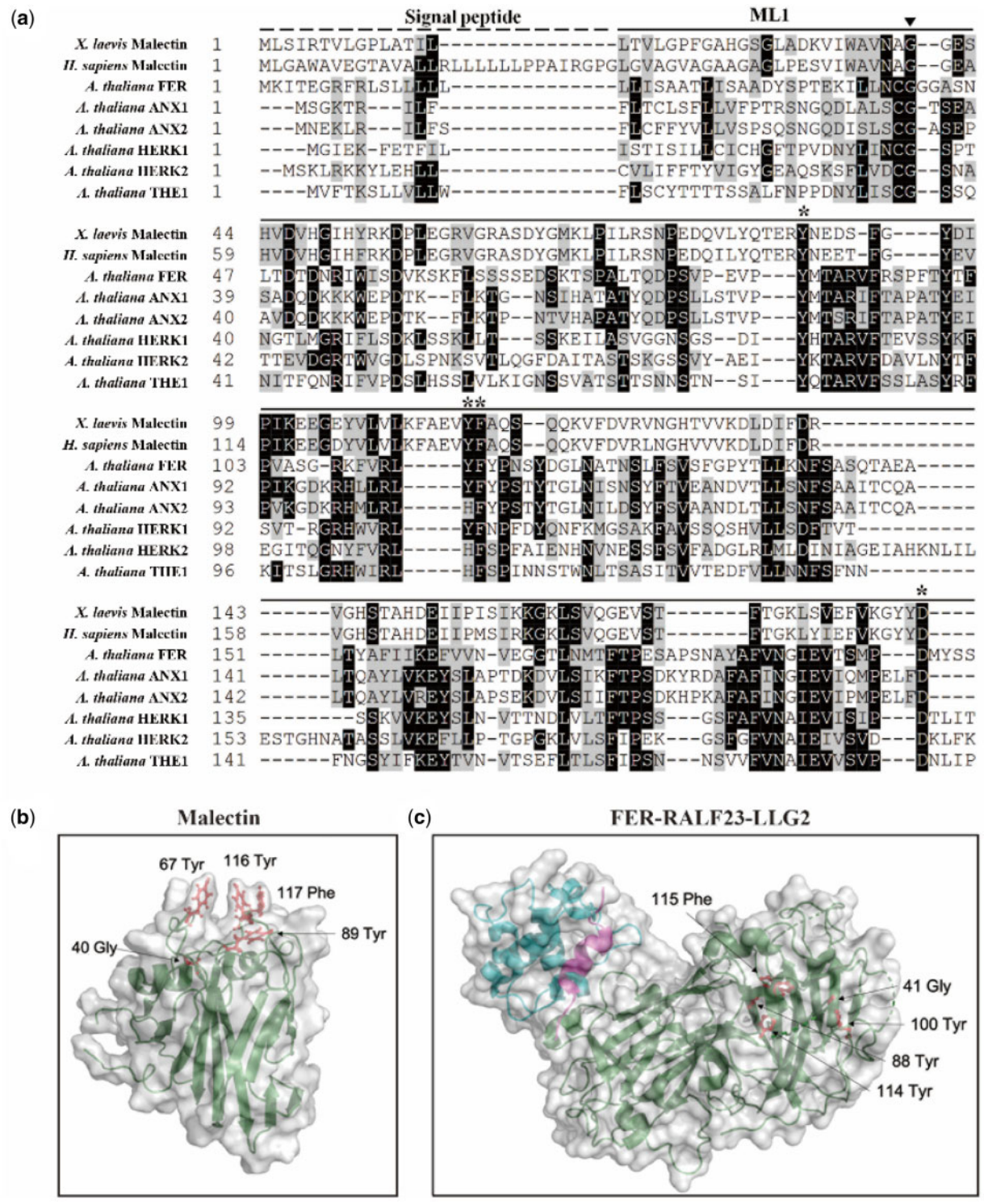

Figure 5 Localization of the highly conserved glycine mutation in *fer-ts* in Arabidopsis FERONIA:RALF23:LLG2 and *X. laevis* malectin structures. (**A**) Several residues important for binding carbohydrate ligands are conserved in plant CrRLK1L receptor kinase family members. Sequences analyzed include animal Malectin (*X. laevis* and *Homo sapiens*) FERONIA and other well-characterized CrRLK1L homologs in Arabidopsis (ANXUR1; ANX1, ANXUR1; ANX2, HERCULES1; HERK1 and THESEUS1; THE1). Putative N-terminal SPs are indicated as black dashed lines and malectin and CrRLK1L ML1 domains by solid lines, respectively. The highly conserved G41 of FER is marked by an arrowhead. Black boxes indicate fully conserved residues; shaded boxes indicate similar and partially conserved residues. Conserved residues that have been shown to participate in binding nigerose in the *X. laevis* malectin structure are marked by asterisks. Sequence alignment analysis was performed by CLUSTAL Omega program (http://www.ebi.ac.uk/Tools/msa/clustalo/) and displayed by using BOXSHADE software (www.ch.embnet.org/software/BOX_form.html). (**B**) Crystal structure of the *X. laevis* malectin protein (PDB ID: 2K46) with binding pocket aromatic residues and the highly conserved glycine residue based on sequence similarity to FER shown in red. C, Crystal structure of FER protein (green) in complex with RALF23 ligand (magenta) and glycosylphosphatidylinositol-anchored protein LLG2 (blue) (PDB ID: 6A5E). No analogous binding pocket is observed on the ML1 domain, as all conserved aromatic residues (red) are buried within the protein. Both (**B** and **C**) were generated using PyMol (DeLano Scientific).

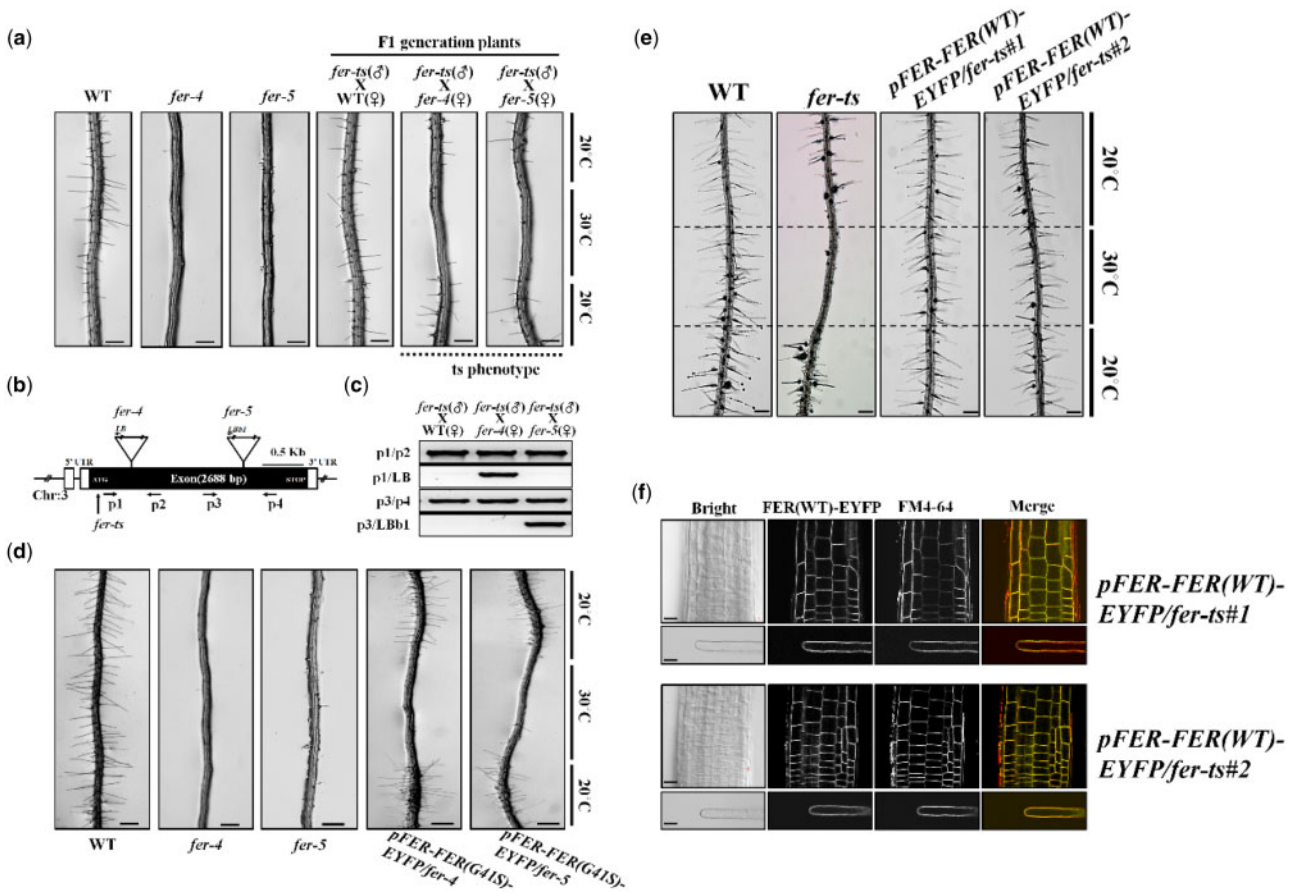

Figure 6 The *fer-ts* mutant confers ts-root hair growth defects when crossed with *fer-4* and *fer-5* mutants. (**A**) WT, *fer-4*, *fer-5*, and F1 progeny from crosses (paternal = *fer-ts*, maternal = *fer-4* or *fer-5*) of *fer-ts*/*fer-4* and *fer-ts*/*fer-5* were grown vertically for 7 d at 20°C, transferred to 30°C for 6 h, and then grown for an additional 24 h at 20°C. Both *fer-ts*/*fer-4* and *fer-ts*/*fer-5* progeny clearly demonstrated a ts-dependent root hair phenotype. Scale bars = 200 μm. (**B**) Schematic diagram of the *FERONIA* gene structure. Open and filled boxes indicate untranslated regions and exon regions, respectively. The locations of T-DNA insertion mutants (*fer-4* and *fer-5*) and *fer-ts* are indicated by triangles and arrows, respectively. (**C**) Genotyping of crossed F1 plants. Genomic DNA was extracted from F1 generation plants and subjected to PCR to confirm the presence of the *fer-4* and *fer-5* genotypes. (**D**) Both *fer-4* and *fer-5* display temperature-dependent root hair phenotypes when transformed with a fluorescently tagged FER construct containing the *fer-ts* mutation (pFER-FER(G41S)-EYFP). Seven-day old seedlings stably transformed and homozygous for (pFER-EYFP(G41S)-EYFP) were grown vertically at 20°C, transferred to 30°C for 6 h, and then grown for an additional 24 h at 20°C. The presence of the transgenic pFER-FER(G41S)-EYFP construct clearly demonstrated a ts-dependent root hair phenotype. Scale bars = 200 μm. (**E**) Temperature-sensitive root hair growth defects of *fer-ts* are fully rescued when transformed with a fluorescently tagged FER construct (pFER-FER(WT)-EYFP). Seven-day old seedlings stably transformed and homozygous for (pFER-EYFP(WT)-EYFP) were grown vertically at 20°C, transferred to 30°C for 6 h, and then grown for an additional 24 h at 20°C. Bright field images were collected with a Nikon Eclipse E600 wide-field microscope with a 10× Plan Apo DIC (0.75 NA) lens. Scale bars = 200 μm. (**F**) Subcellular localization of FER(WT)-EYFP protein in roots and root hairs in a rescued *fer-ts* mutant plant. Fluorescent confocal images displaying the subcellular distribution of FER(WT)-EYFP protein was detected from growing root, and mature root hair cells of 7-d-old *fer-ts* seedlings stably transformed and homozygous for pFER-FER(WT)-EYFP. Cells were counter-stained by incubating for 5 min in FM4-64 to visualize cell membranes. Images were collected by spinning-disk fluorescence confocal microscopy using a Zeiss 40× Plan-Apochromat (1.3 NA) lens with appropriate EYFP and FM4-64 fluorescence filter sets. Scale bars = 10 μm.

continuous incubation at elevated temperatures *fer-ts* mutant proteins also appear to be subject to enhanced protein turnover.

The *fer-ts* mutant displays impaired sensitivity to RALF1 peptides in elevated temperature conditions

Signaling in the CrRLK1L family of receptor kinases have been linked to a family of small extracellular peptide hormones called RALFs (Haruta et al., 2014; Stegmann et al., 2017). RALF1, which was previously demonstrated to suppress cell elongation of the primary root in Arabidopsis and other plants (Pearce et al., 2001), has now been shown to directly bind with the FER extracellular domain (Haruta et al., 2014; Stegmann et al., 2017). Because the G41S mutation in *fer-ts* appears to rapidly inhibit tip-restricted growth at elevated temperatures, perhaps by destabilizing the structure of the extracellular domain of this protein (Figure 8f), we were curious what effect RALF1 peptides might have on root hair growth, and whether the *fer-ts* mutant may display altered responses to RALF1 peptide treatments at elevated

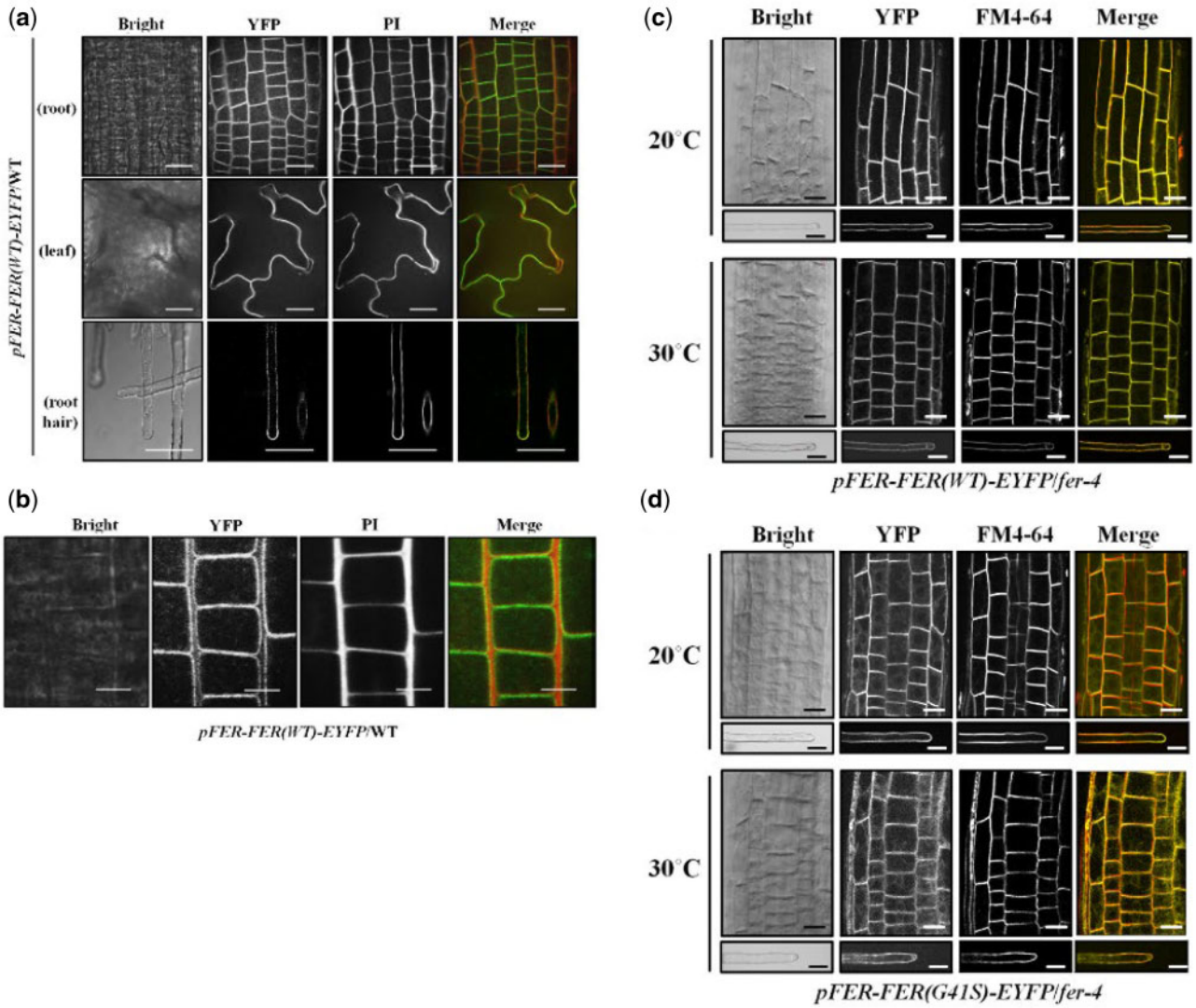

Figure 7 Subcellular localization of FER(WT)-EYFP and FER(G41S)-EYFP fluorescent fusion proteins in stably transformed Arabidopsis. (**A**) Subcellular localization of FER(WT)-EYFP protein in various tissues. Fluorescent confocal images displaying the subcellular distribution of FER(WT)-EYFP protein were detected from growing root, leaf and root hair cells of 7-d-old seedlings in *pFER-FER(WT)-EYFP*/WT transgenic plants. Cell walls were counter-stained by incubating for 5 min in a PI solution (10 μg/ml). Images were collected by spinning-disk fluorescence confocal microscopy using a Zeiss 40× Plan-Apochromat (1.3 NA) lens with appropriate EYFP and PI fluorescence filter sets. Scale bars = 20 μm. (**B**) Magnified images of FER(WT)-EYFP fluorescence. FER(WT)-EYFP in WT of growing root cells of 7-d-old Arabidopsis seedlings was detected by spinning-disc confocal microscopy using a Zeiss 100× Plan-Apochromat (1.46 NA) oil immersion objective with appropriate EYFP and PI filter sets. Scale bars = 10 μm. (**C** and **D**) Subcellular localization of FER(WT)-EYFP (**C**) and FER(G41S)-EYFP (**D**) fluorescent fusions in root and root hair cells at normal (20°C) and elevated (30°C) temperatures. Cells from *fer-4* plants stably transformed and homozygous for FER(WT)-EYFP or FER(G41S)-EYFP were counterstained with FM4-64 (5 μM) for 5 min to visualize cell membranes. Images were collected by spinning-disk fluorescence confocal microscopy using a Zeiss 40× Plan-Apochromat (1.3 NA) lens with appropriate EYFP and FM4-64 fluorescence filter sets. Scale bars = 20 μm; root, 10 μm; root hair.

temperatures (30°C). Treatment of growing *fer-ts* and WT (Figure 9A and Supplemental Movie S4) root hairs resulted in rapid cessation of tip-growth (<1 min; Figure 9B) in normal temperatures (20°C).

Because *fer-ts* root hair growth was already inhibited at 30°C it was not possible to measure RALF1 peptide effects in root hair cells. However, since primary root elongation did not appear to be as dramatically affected at elevated temperatures as root hair growth (30°C; Supplemental Figure S1), we examined the temperature-dependent effect of RALF1 peptide treatment on these tissues. As shown in Figure 10, both WT seedlings and *fer-ts* mutants were highly sensitive to active RALF1 peptide under normal temperature conditions (20°C). However, as previously described, the sensitivity of root growth to RALF1 in the *fer-5* mutant was reduced in comparison to WT plants at 20°C (Figure 10A and C). Importantly, sensitivity of *fer-ts* seedlings to RALF1 peptide treatment was dramatically reduced at 30°C, even though WT plants and *fer-5* mutants still responded to RALF1 peptide treatment with similar levels of root

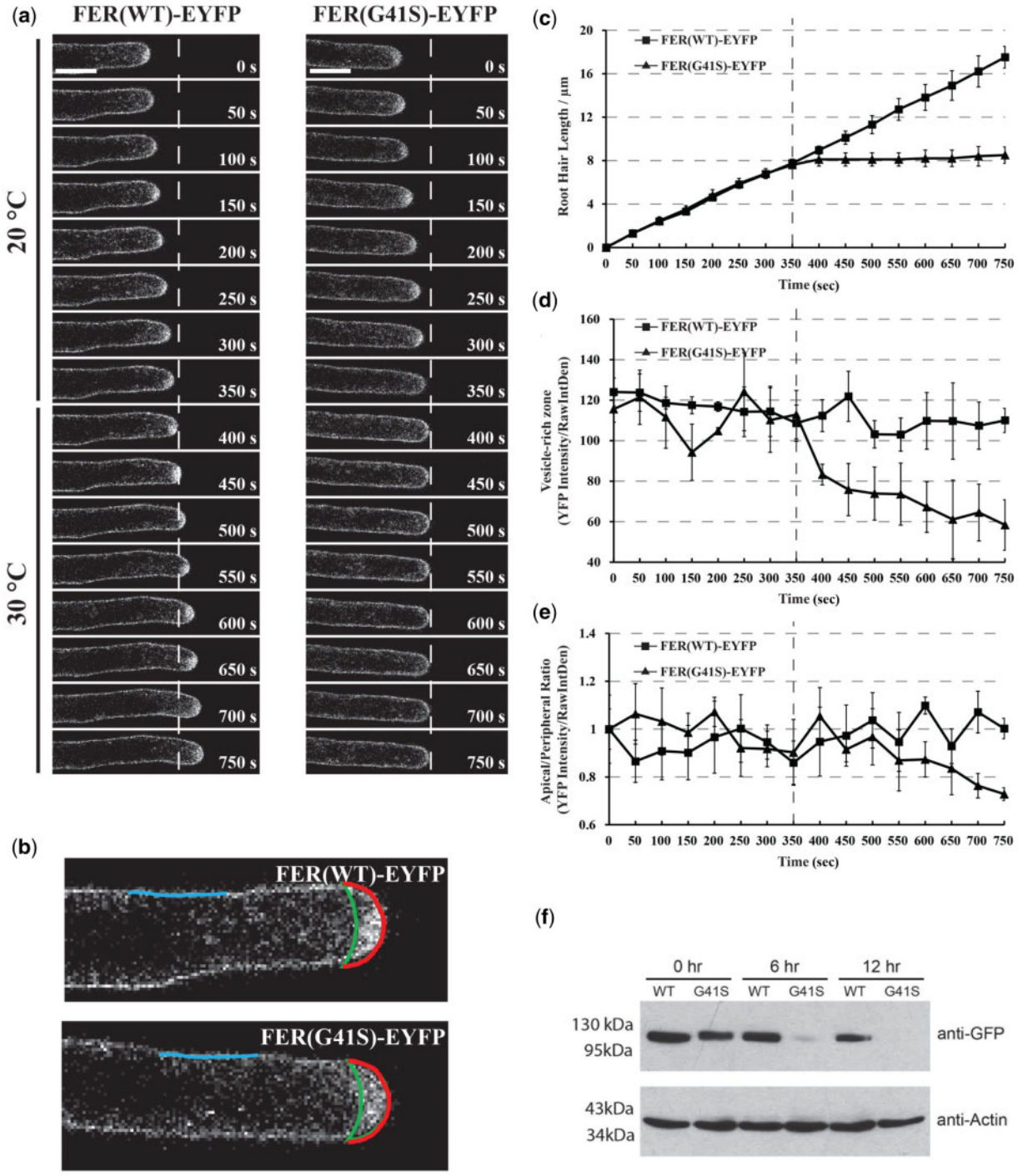

Figure 8 Subcellular localization dynamics of FER(WT)-EYFP and FER(G41S)-EYFP proteins in growing root hair cells under both normal (20°C) and elevated (30°C) temperatures. (**A**) Root hair tip-growth in stably transformed lines expressing FER(WT)-EYFP and FER(G41S)-EYFP fluorescent fusion proteins under (20°C) and (30°C) temperature by time-lapse microscopy. Confocal images were acquired using a Leica confocal laser-scanning microscope SP8 with a 63× oil lens (Numerical Aperture = 1.4) with 5 s intervals. Representative images are presented at 50 s intervals (10 frames). Scale bar: 10 μm. (**B**) Schematic diagram showing areas and lines used for fluorescence intensity quantification. Apical (red line) and peripheral (blue line) plasma membrane domains were measured, and the area between the apical plasma membrane and green line represents the vesicle-rich zone. (**C**) Quantitative analysis of root hair growth in stably transformed lines expressing FER(WT)-EYFP (n = 3) and FER(G41S)-EYFP (n = 3). Root hair elongation was measured every 50 s using the measurement function in ImageJ. (**D**) Quantitative analysis of YFP intensity of the vesicle-rich zone. (**E**) Quantitative analysis of YFP intensity of the apical/peripheral ratio. Values are normalized using 0 s as 100%. The dashed line indicates the time point of transition from permissive (20°C) to (30°C). Error bars in (**C**–**E**) represent SD. (**F**) Protein turnover rates of FER(WT)-EYFP and FER(G41S)-EYFP at elevated temperature (30°C). Five-day-old seedlings were grown at 20°C and then treated with 200 μM cycloheximide and transferred to 30°C. Total proteins were extracted at each time point and the relative levels were determined using immunoblotting with anti-GFP and anti-actin antibodies. FER(G41S)-EYFP levels rapidly decreased during the time course, while levels of FER(WT)-EYFP were not significantly reduced. Actin was used as a loading control.

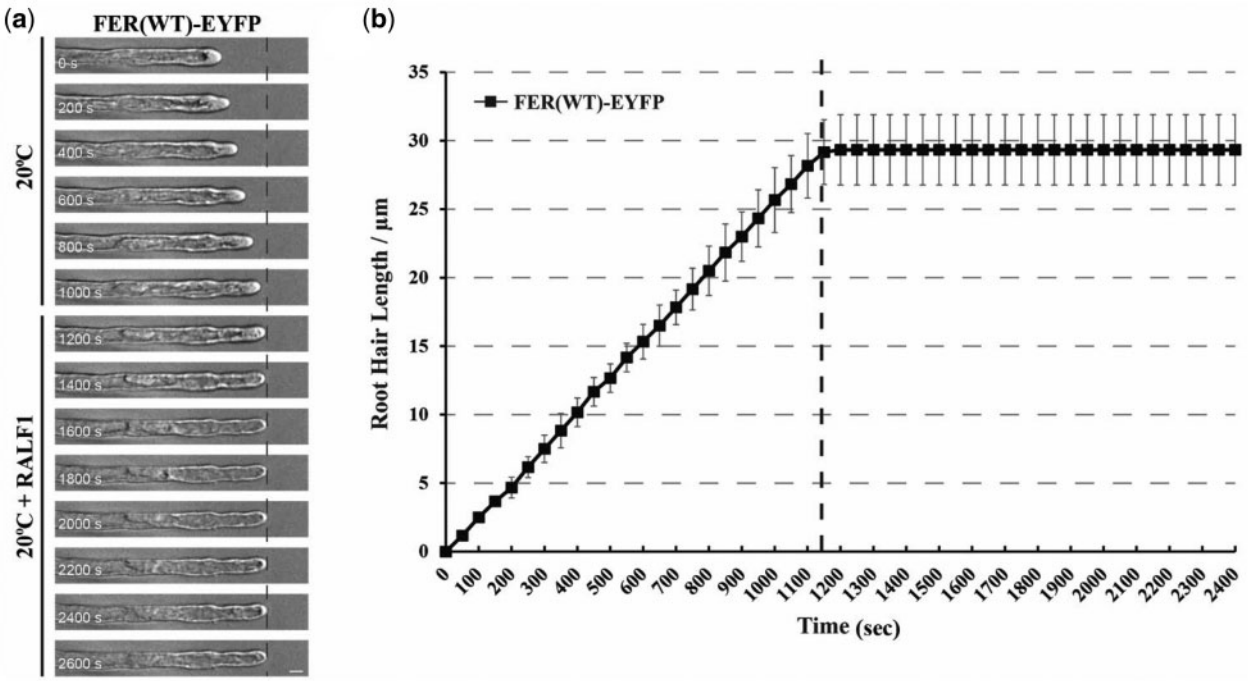

Figure 9 RALF peptide treatment terminates root hair growth in the FER(WT)-EYFP expressing line. (**A**) Root hair tip-growth in stably transformed lines expressing the FER(WT)-EYFP fluorescent fusion protein under permissive (20°C) temperature by time-lapse microscopy. Bright field images of growing root hair cells (n = 3) were collected using a Nikon Eclipse E600 wide-field microscope with a ×20 Plan Apo (0.45 NA) lens with 5 s intervals. The dashed line represents when media containing RALF1 (1 μM) was perfused into the growth chamber. Representative images are presented at 200 s intervals. Scale bar: 50 μm. (**B**) Quantification of root hair growth. Root hair elongation was measured every 50 s using the measurement function in ImageJ. Error bars represent SD.

elongation inhibition (Figure 10B and D). These results support the previous determination that RALF1 peptide signaling occurs through the FER RLK during root elongation, and would be consistent with the G41S mutation resulting in temperature-sensitive inhibition of RALF1-mediated FERONIA signaling. However, the rapid loss of tip-growth at 30°C even in the absence of added RALF1 peptide might indicate a separate signaling role for FER during tip-growth in root hair cells.

ROS accumulation of the *fer-ts* mutant was greatly reduced at 30°C and the *fer-ts* phenotype was not rescued by various hormone treatments

In previous reports, ROS accumulation is highly reduced in *fer-4* and *fer-5* mutants especially in root hair tips and primary roots (Duan et al., 2010). In order to investigate the ROS accumulation, WT and *fer* mutants were treated with 2′,7′-dichlorodihydrofluorescein diacetate (H_2DCF-DA) to monitor ROS levels. In WT plants, ROS accumulation was observed in primary roots and root hairs, and in root hairs these levels increased slightly upon 1-naphthaleneacetic acid (NAA) treatment at both 20°C and 30°C (Figure 11). While *fer-ts* plants showed similar ROS accumulation patterns as those observed in WT plants at 20°C, at 30°C ROS accumulation was dramatically reduced both in the absence and presence of NAA (Figure 11A). However, while ROS accumulation in the *fer-ts* mutant was strictly temperature dependent (compare Figure 11B and C), these reduced ROS levels were similar to those observed at both temperatures for the constitutive *fer-4* and *fer-5* mutants (Figure 11A; compare Figure 11B and C).

In order to investigate how broadly the temperature-sensitive *fer-ts* mutant phenocopied *fer-4* and *fer-5* mutants, these three mutants were treated with several different concentrations of hormones, and then root hair lengths and densities were measured either at 20°C or 30°C. Root hair lengths and densities displayed similar patterns for both WT and *fer-ts* plants at 20°C, while both *fer-4* and *fer-5* root hairs were consistently shorter and less dense (Supplemental Figure S5a and S5b; upper panels). However, at 30°C, *fer-ts* root hair lengths and densities largely resembled the *fer-4* and *fer-5* phenotypes (Supplemental Figure S5a and S5b; lower panels). Primary root length, total lateral root number, fresh weight, and total leaf numbers of *fer-ts* mutants also displayed a similar temperature-dependent trend; resembling WT plants with various hormone treatments at 20°C, but resembling *fer-4* and *fer-5* mutants at 30°C (Supplemental Figure S6).

Discussion

In eukaryotes, RLKs have been implicated to play an important role in many crucial eukaryotic cellular processes, such as cell cycle progression, cell signaling, embryogenesis, and abiotic and biotic stress responses (Shiu and Bleecker, 2001;

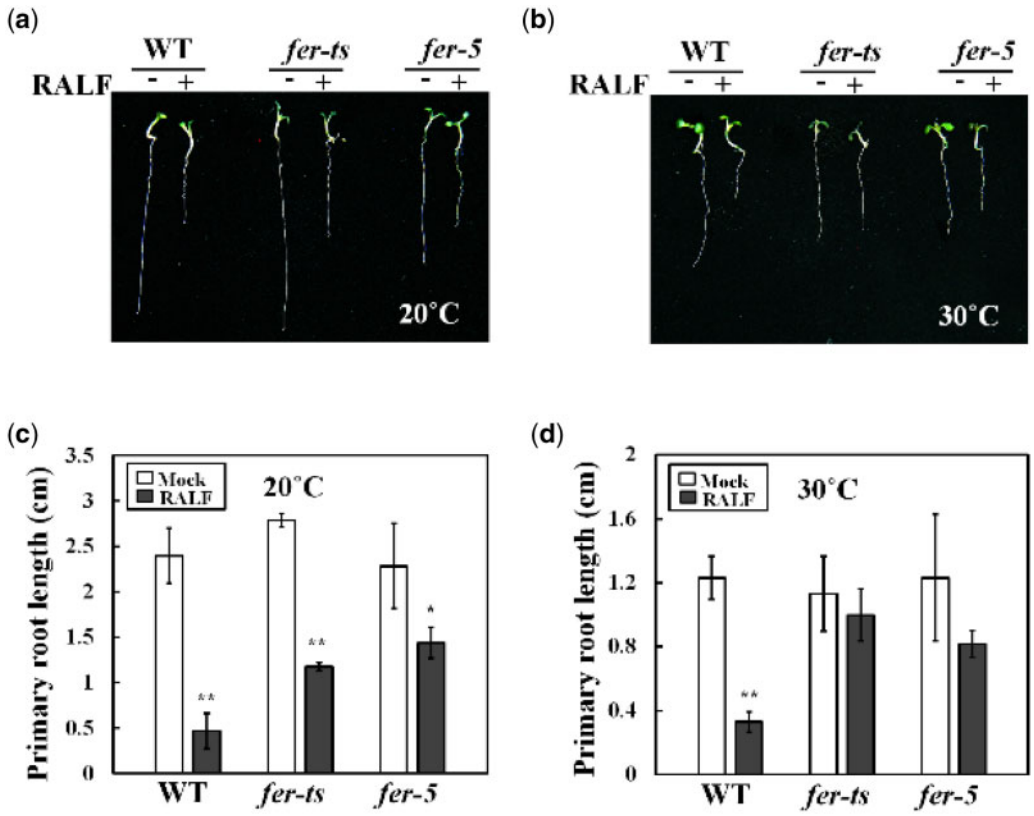

Figure 10 *fer-ts* mutants are partially insensitive to RALF1 peptide-mediated root growth inhibition at elevated temperatures. WT, *fer-ts*, or *fer-5* plants were germinated and grown for 3 d in 1/2 MS liquid media at 20°C, and then transferred to 1/2 MS liquid media containing 1 μM RALF1 peptide (RALF +) or a mock buffer control (RALF−) and grown an additional 3 d at 20°C (A) or 30°C (**B**). Images of representative seedlings were collected using an Olympus SZX12 stereoscopic microscope. Quantification of primary root lengths (n = 10 seedlings) in the presence or absence of RALF1 peptide treatment in normal, 20°C (**C**) and elevated, 30°C (**D**) conditions. Primary root lengths were determined using Image J. Error bars represent SD. *$P < 0.05$, **$P < 0.01$ by Student's t test.

Morillo and Tax, 2006; Lehti-Shiu et al., 2009). In this study, we isolated and identified a temperature-sensitive root hair elongation mutant, which we have determined is a new mutant *FER* allele that we have called *fer-ts*. The *fer-ts* mutant displays normal overall growth characteristics at normal temperature (20°C), but root hair initiation and elongation are specifically and rapidly inhibited within 1 min upon transfer of these plants to elevated temperature (30°C). We have shown that the *fer-ts* mutant is the result of a substitution mutation in which a highly conserved glycine residue in the FER extracellular domain is changed to serine (G41S). FERONIA is a member of the CrRLK1L subfamily of RLKs in Arabidopsis and the mutated glycine residue (G41S) is highly conserved in multiple members of the CrRLK1L family of receptor proteins as well as in animal malectin proteins.

While both FER(WT)-EYFP and FER(G41S)-EYFP fusion proteins displayed a plasma membrane localization at both normal and elevated temperatures, FER(G41S)-EYFP displayed significantly increased protein turnover at 30°C (Figure 8). However, this increased protein turnover did not appear to result in loss of accumulation of FER(G41S)-EYFP in plasma membranes. This is likely due to ongoing protein synthesis and at least some secretion of these proteins at the elevated temperature. These results, along with the rapid cessation of root hair elongation (<1 min) in elevated temperatures would be consistent with rapid inactivation of FER signaling activity due to protein inactivation rather than simply depletion of FER activity from the plasma membrane due to increased turnover.

FER has been implicated in a variety of plant processes, including roles in root hair tip growth as well as crucial plant processes, such as pollen tube reception, hypocotyl elongation, regulation of abscisic acid signaling, and controlling seed size (Escobar-Restrepo et al., 2007; Deslauriers and Larsen, 2010; Duan et al., 2010; Yu et al., 2012, 2014). In many of these processes, FER signaling appears to regulate ROS production. In constitutive *fer* mutants, ROS levels are reduced, and FER overexpression results in increased ROS levels. The observation that the *fer-ts* mutant also displays reduced ROS levels only at elevated temperatures suggests that this mutation affects FER signaling in a similar fashion as other *fer* mutants, perhaps providing a powerful tool for elucidation of downstream signaling events associated with FER function, and indicating that at least one important downstream effect of *FER* signal transduction is regulation of ROS production. This was elegantly explained by the discovery that FER recruits ROPGEFs, which in turn activate ROP GTPases, leading to the stimulation of RHD2 NADPH

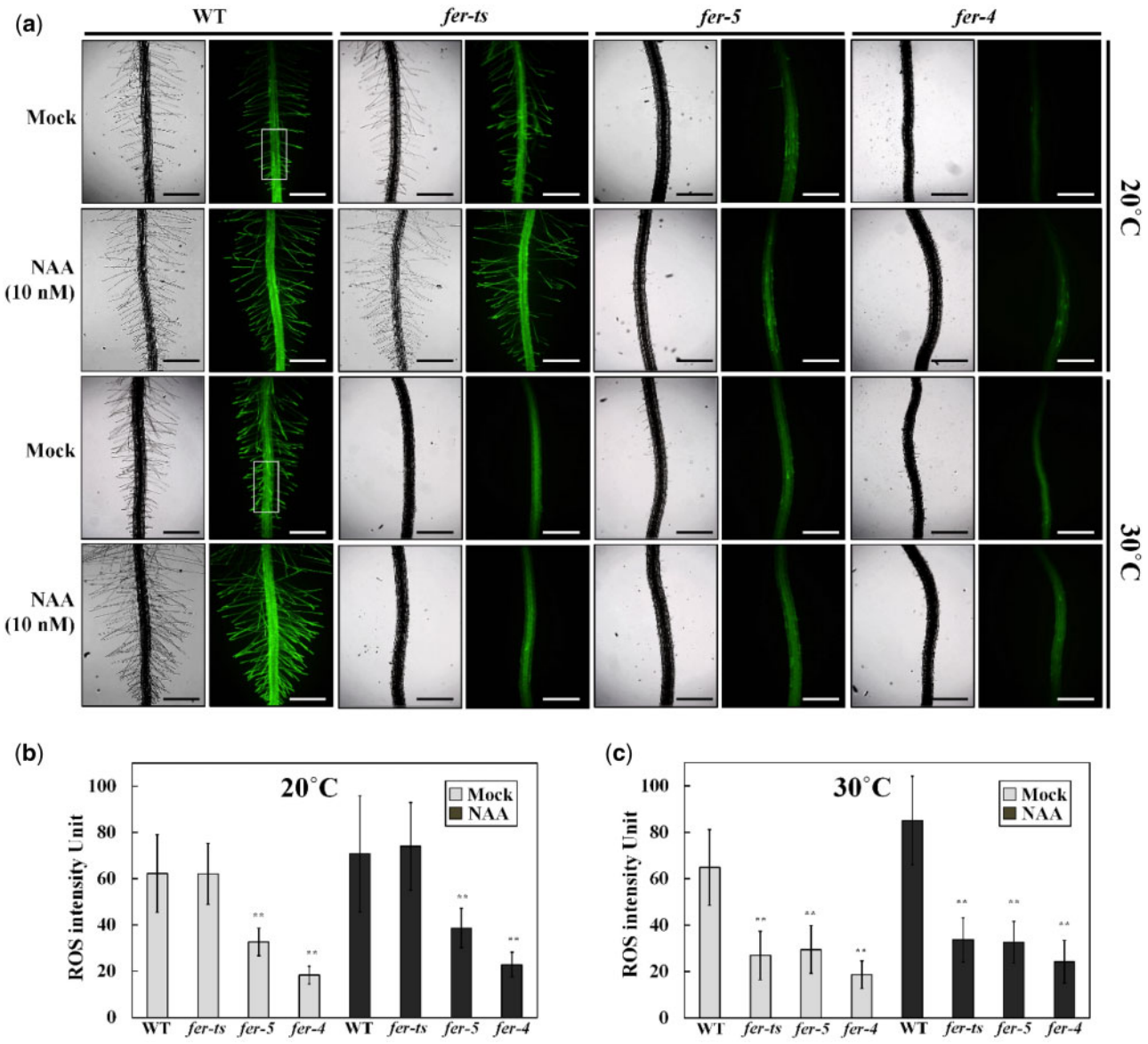

Figure 11 Detection of ROS in WT, *fer-ts* and *fer-5* primary roots and root hairs. (**A**) ROS accumulation in normal and elevated temperature conditions with or without auxin treatments. WT, *fer-ts*, *fer-4*, or *fer-5* seedlings were grown vertically on 1/4 MS media plates for 7 d at normal (20°C) or elevated (30°C) temperatures in the presence or absence of 10 nM NAA. Plates were bathed with 5 mL of 50 μM in H_2DCF-DA suspended in 1/4 MS liquid media for 5 min, followed by two gentle washes with 10 mL of 1/4 MS. Fluorescence images were collected with a Zeiss Axio Imager Z1 fluorescence microscope with 2.5× objective and green (GFP) filter set. The WT ROS image was acquired by auto-exposure and all other images were acquired using the WT exposure conditions. Scale bars = 500 μm. (**B and C**) The rectangle in (**A**) indicates a representative ROI where average ROS intensity was quantified for the samples at 20°C (**B**) and 30°C (**C**). Intensities of ROS were quantified by image J program. Error bars represent SD. ** $P < 0.01$ by Student's *t* test.

oxidase-dependent ROS production (Duan et al., 2010). Therefore, FER-mediated regulation of ROS production is likely important and tightly controlled for many cellular functions.

Based on sequence comparison, the extracellular domains of members of the CrRLK1L subfamily of plant RLK proteins were predicted to share some structural similarity to the mammalian malectin protein (Schallus et al., 2008). Malectin was first identified and characterized in *X. laevis* as a carbohydrate binding protein in the endoplasmic reticulum where it plays an important role in the early steps of protein N-glycosylation for biogenesis of glycoproteins (Schallus et al., 2008). Based on nuclear magnetic resonance structure analysis, there are five key residues in the malectin domain (Y67, Y89, Y116, F117, D186) that are located in a pocket-shaped structure, and these aromatic residues and the aspartate mediate interactions with the glucose residues of maltose and nigerose di-saccharide ligands (Schallus et al., 2008). In plants, malectin-like domains are mainly found in the CrRLK1L subfamily and these display low overall sequence identity with animal malectins (Shiu and Bleecker, 2003). In FER, two malectin-like domains, ML1 and ML2, are found as

a tandem-repeat in the extracellular domain. Interestingly, several key residues found in the ligand-binding pocket of the animal malectin structure are maintained in the malectin-like domains of FER and other plant CrRLK1L family members (Schallus et al., 2008). However, the discovery that members of a family of small secreted peptides, RALFs, rather than cell wall polysaccharides or oligosaccharides, serve as important ligands for FER and other CrRLK1L family receptors (Haruta et al., 2014; Ge et al., 2017; Stegmann et al., 2017; Gonneau et al., 2018) might indicate that these extracellular domains may interact with ligands in a manner distinct from their animal counterparts. Indeed the recent structural characterization of ANX1/2 extracellular domains (Du et al., 2018) and the FER extracellular domain in complex with RALF23 and the FER co-receptor, LLG2 (Xiao et al., 2019) has shown that the RALF23 binding domain and interaction with LLG2 occurs primarily with the ML2 domain, and that conserved tyrosine and phenylalanine residues in CrRLK1L malectin folds in these structures appear to be buried within the ML1 fold, and therefore likely unavailable to interact with cell wall carbohydrates in a manner similar to animal malectins.

On the other hand, analysis of the animal and plant malectin domains reveals an additional invariant glycine residue that is present in all animal and plant malectin sequences, and which is also found in close proximity to a pocket-shape ligand-binding cleft determined in the structure of the animal malectin protein. This invariant glycine is replaced with a serine (G41S) in the *fer-ts* mutation described in this paper. The highly conserved nature of this glycine residue, and the rapid elimination of FER signaling at elevated temperatures, suggests a critical role for the FER ML1 domain in ligand binding or transduction of a ligand-binding signal in members of the CrRLK1L family of RLKs. Indeed, mutation of an analogous glycine residue to aspartic acid (G37D) in the extracellular domain of THESEUS in the *the1-1* mutant also results in a loss of function mutation in this RLK (Hematy et al., 2007). The *the1-1* mutation also results in its insensitivity to its specific RALF ligand, RALF34 in vivo (Gonneau et al., 2018). However, RALF34 was still found to bind the extracellular domain of *the1-1* containing the G37D mutation in vitro, suggesting that mutation of this glycine residue did not directly impact RALF34 binding (Gonneau et al., 2018). Similarly, the response of the *fer-ts* mutant to treatment with RALF1 peptide was dramatically reduced under elevated temperature conditions (Figure 10). Precisely, how the G41S *fer-ts* mutation, which is not found within the RALF23 peptide binding surface in the FER ML2 domain, would directly block RALF peptide perception and signaling is unclear, although it should be noted that the timescales of root growth analysis (>6 h) are substantially longer and therefore the increased protein turnover of *fer-ts* receptors (Figure 8F) may play a role not observed in the rapid cessation of tip-growth in root hairs (<1 min).

Additionally, the rapid cessation of tip-growth in *fer-ts* root hairs occurs even in the absence of added RALF1 peptide, perhaps indicating non-RALF peptide mediated signaling by FER receptor proteins. The recent discovery of links between *FER* signaling and pectin dynamics during salt stress (Chen et al., 2016; Feng et al., 2018) and fertilization events (Duan et al., 2020) may provide insight into potential non-RALF peptide mediated signaling by FER and related CrRLK1L family proteins. During salt stress, *FER* appears to sense cell wall softening and both FER ML1 and FER ML2 domains were shown to directly interact with pectin in vitro (Feng et al., 2018). More recently, *FER* function was shown to be required in order to maintain de-esterified pectin levels in the filiform apparatus during pollination and fertilization events (Duan et al., 2020). In addition, other CrRLK1L receptor kinases, such as *ERULUS* (*ERU*; Schoenaers et al., 2018) and *THE1* (Gonneau et al., 2018), also appear to regulate aspects of pectin methyl esterification and cell wall integrity sensing, respectively. Whether the G41S mutation in *fer-ts*, or other analogous mutations of this invariant glycine residue in other CrRLK1L receptors affect the ability of these receptors to interact with or regulate pectin dynamics in plant cell walls is an intriguing possibility that warrants future investigation.

Materials and methods

Plant materials and growth conditions

The *fer-ts* mutant was isolated from an EMS mutagenized population of *A. thaliana* ecotype Columbia (Col-0) stably transformed with a single copy of EYFP-RabAb4 driven by a 35S promoter (Preuss et al., 2004; Weigel and Glazebrook, 2006), and two FERONIA T-DNA insertional mutants (*GABI-GK106A06* (designated as *fer-4*) and *SALK_029056c* (designated as *fer-5*; Duan et al., 2010) were used in this study. Seeds were sterilized by soaking in 1% (v/v) bleach solution for 10 min; after washing five times with sterilized water, they were sown onto agar plates for germination. Five- to seven-day-old Arabidopsis seedlings used in the root hair growth assays were grown vertically on plates containing 0.25× Murashige and Skoog (MS; Sigma-Aldrich) medium at pH 5.7 supplemented with 0.6% (w/v) phytagel at 20°C under long day conditions (16-h d with 150 $\mu E \cdot m^{-2} \cdot s^{-1}$ (E, Einstein; 1 E = 1 mol of photons). For harvesting seeds, seedling plants were transferred to soil and grown to maturity at 20°C under long day conditions.

Quantification of root hair elongation in fer-ts mutants under normal and elevated temperatures

To characterize root hair growth defective phenotypes in the *fer-ts* mutant, bright-field microscopy was carried out using a Nikon Eclipse E600 wide-field microscope with a 10× Plan Apo (0.45 NA) lens as previously described (Preuss et al., 2004). The *fer-ts* mutants were germinated and grown vertically on plates containing 0.25× MS medium at pH 5.7 supplemented with 0.6% (w/v) phytagel at 20°C for 7 d and then transferred to 30°C and grown for 6 h before returning back to 20°C growth conditions for an additional 24 h, when images of roots and root hairs were then collected.

Time-lapse video microscopic analysis was carried out under normal and elevated temperature conditions in WT and *fer-ts* mutants as described previously (Preuss et al., 2004). Images of growing root hairs were collected from seedlings by time-lapse video microscopy either using a Nikon Eclipse E600 wide-field microscope with a 10× Plan Apo (0.45 NA) lens (for bright-field images), or using a Leica confocal laser-scanning microscope SP8 with a 63× oil lens (1.4 NA). YFP fluorescence was excited at 514 nm and visualized from 519 nm to 650 nm (Yang et al., 2020). The temperature of the MS medium was controlled by an inline single-channel automatic temperature controller (Werner Instruments, Hamden, CT, model:TC-324B) controlled by a dry air thermostat inserted into the growth chamber and situated ~2 mm from the region of interest (ROI). Temperatures were actively recorded using an infrared thermometer (Kintrex Inc., Vienna, VA, model:IRT0424). Raw image sequences were cropped with Adobe Photoshop and imported into Fiji-ImageJ (Schindelin et al., 2012) to generate time projections using the Stacks function. Root-hair lengths, growth rates, and densities were quantified by using calibrate and measure functions.

Map-based cloning and full-genome sequencing of *fer-ts*

Self-fertilized, backcrossed *fer-ts* (ecotype; Columbia) mutants were crossed with Landsberg WT plants to generate a mapping population. F_1 crossed plants were checked for heterozygosity with the SSLP marker "nga8" that is polymorphic between Col-0 and L*er* (Bell and Ecker, 1994). Homozygous *fer-ts* plants were selected from the segregating F2 population by germination on MS media plates at 20°C, and root hair tip growth defective phenotypes in elevated growth temperatures (30°C) were analyzed. Homozygous plants displaying *fer-ts* phenotypes were grown to maturity at 20°C and seed were collected. Genomic DNA was isolated using Qiagen Plant DNA mini kits, and SSLP markers were used for rough mapping the *fer-ts* mutant lesion, which was initially located on chromosome 3 between the SSLP markers *NIT 1.2* and *NGA6*. Low-resolution mapping narrowed the location of the *fer-ts* mutant locus to ~2 Mb region of chromosome 3, and full genome sequencing was performed to further determine the *fer-ts* mutation within this region. Libraries were generated for both the *fer-ts* and WT (ecotype Columbia) extracted DNA using Illumina TruSeq DNA kits and barcoded for multiplexing by the University of Michigan DNA Sequencing Core. Samples were sequenced on an Illumina MiSeq platform with paired-end 150 bp cycles. Sequence reads were checked for quality using FastQC then aligned to the TAIR9 genome using Bowtie2. Potential SNPs were identified using Freebayes. Additional analysis of sequence variants within the low-resolution mapped 2 Mb region of chromosome 3 to eliminate SNPs common to our re-sequenced Col-0 population and the *fer-ts* allele were sorted for context and predicted effect using a custom PERL script.

Fluorescence microscopic analysis

For pFER-FER(WT)-EYFP and pFER-FER(G41S)-EYFP transgenic plants, the full length of *FERONIA* including the ~2 kb promoter was prepared by PCR reaction and sub cloned into the pCAMBIA-EYFP-C1 expression vector (Preuss et al., 2004). WT and mutant FERONIA sequences were amplified from genomic DNA isolated from WT and *fer-ts* mutant plants using PCR. To produce pFER-FER(WT)-EYFP and pFER-FER(G41S)-EYFP transgenic plants, these constructs were introduced into *Agrobacterium tumefaciens* strain GV3101, and Arabidopsis plants were transformed with *A. tumefaciens* using the "floral-dip" method (Clough and Bent, 1998). Transgenic plants for each construct were selected by germination on 25 mg/L of hygromycin-containing medium (Duchefa, Haarlem, The Netherlands) under long day conditions (16 h light/8 h dark cycle) at 20°C. Three or more independent, homozygous transgenic lines were isolated for each of the pFER-FER(WT)-EYFP and pFER-FER(G41S)-EYFP constructs in the *fer-ts*, *fer-4*, and *fer-5* mutant backgrounds, respectively, and a single representative homozygous line was used in these studies. Confocal images were generated using a laser confocal microscope (Zeiss Observer.A1) connected to a CSU10 confocal scanner unit (Yokogawa, Japan) and a 10× Plan-Neofluar (0.3 NA lens), 40× Plan-Apochromat (1.3 NA lens), or 100× Plan-Apochromat (1.46 NA lens) oil objective with 491 nm laser excitation and a 535 nm emission filter for EGFP and EYFP fluorescence. To visualize cell walls, seedlings were incubated for 5 min in propidium iodide (PI, 10 μg/mL) and then washed with 0.25× MS media, and then cell membranes were stained with FM 4-64 (5 μM) for 5 min before washing with 0.25× MS media. Images were collected with a Hamamatsu C9100-50 camera operated using the Volocity software version 5 [the electron-multiplying (EM)-CCD detector gain settings were 123, 116, and 190 for images collected with 10×, 40×, and 100× objectives, respectively].

RT-PCR analysis

For detection of *FERONIA* expression, WT, *fer-4*, *fer-5*, and *fer-ts* plants were frozen immediately in liquid nitrogen. Two microgram aliquots of total RNA extracted from the WT or mutant seedlings were used for reverse transcription primed by oligo(dT). Superscript III (Invitrogen, USA) was used for the reverse transcription reaction according to the manufacturer's instructions. One-microliter aliquot of the reaction mixture was used for subsequent PCR analysis. *Actin* was used as a quantifying control.

Detection of ROS in roots

ROS detection by using H_2DCF-DA in root hairs and primary roots was performed following the protocol described previously (Duan et al., 2014). Briefly, Arabidopsis seedlings were germinated and grown vertically on 0.25× MS media plates for 7 d at normal (20°C) or elevated (30°C) temperatures. Plates were bathed with 5 mL of 50 μM in H_2DCF-DA (Sigma-Aldrich) suspended in 0.25× MS liquid media for 5 min, followed by two gentle washes with 10 mL of 0.25×

MS. Fluorescence images were collected with a Zeiss Axio Imager Z1 fluorescence microscope with a 2.5× objective and green (GFP) filter set.

Effect of RALF1 peptide on root hair and root growth inhibition

Synthetic Arabidopsis RALF1 polypeptide was synthesized by using 9-fluorenylmethyl chloroformate solid-phase chemistry with a peptide synthesizer from Thermo Scientific company and confirmed by MALD-TOF analysis (Applied Biosystems Voyager System 2098, USA). After synthesis, 5 mg of reduced synthetic polypeptide was oxidized by dissolving in 25 mL of degassed 0.1 M ammonium bicarbonate and incubating for 2 d in an opened flask under 4°C, then lyophilized. Lyophilized RALF1 powder was re-suspended in 10 mL of PBS buffer followed by two buffer exchange steps using Amicon Ultra centrifugal filter (Ultracel-3K, 3000*g* for 45 min each) to remove any residual ammonium bicarbonate. Seedling germination was performed in 0.5× MS liquid medium at 20°C for 3 d in long-day conditions (16-h d with 150 $\mu E \cdot m^{-2} \cdot s^{-1}$ (E, Einstein; 1 E = 1 mol of photons) light intensity. After 3 d, germinated Arabidopsis seeds were transferred to six-well Falcon tissue culture plates with 3 mL of 1/2× MS liquid media containing 1 μM RALF1 or an equal volume of PBS and agitated on a shaker at 100 rpm (Model VS201D, Vision Scientific CO., LTD) for an additional 3 d at 20°C or 30°C. All solutions were filter-sterilized (0.2 μm pores, Minisart 16534), and the seedlings were photographed 3 d after being transferred to the media. Quantification of primary root length was measured using ImageJ software. Time-lapse video microscopic analysis was carried out under permissive temperature conditions in WT. 0.25× MS liquid media with/without 1 μM RALF1 peptide were pumped into the chamber while imaging. All solutions were filter-sterilized (0.2 μm pores, Minisart 16534).

Statistical analysis

All experiments were performed in triplicate. Error bars show the SD of three (or more, as indicated) replicates. Values are means ± SD of three (or more) independent biological replicates. Significant differences were detected by Student's *t* test using Excel software. Differences were considered significant at $^{*}P < 0.05$ and $^{**}P < 0.01$ (or $^{**}P < 0.001$ in Figure 1).

Accession numbers

Sequences of the genes in this paper may be found in the GeneBank/EMBL database library under the following accession numbers: At3g51550 (FER), At4g39990 (RabA4b), At3g18780 (Actin2), At3g04690 (ANX1), At5g28680 (ANX2), At3g46290 (HERK1), At1g30570 (HERK2), At5g54380 (THE1), NP_001085212.1 (*X. laevis* Malectin), NP_055545.1 (*Homo sapiens* Malectin).

Supplemental data

Supplemental Figure S1. Primary root growth of *fer-ts* mutants under normal and elevated temperature conditions.

Supplemental Figure S2. Root hair growth chamber temperature measurement during transition from normal (20°C) to elevated (30°C) temperature conditions.

Supplemental Figure S3. Sequence alignment of Arabidopsis CrRLK1L subfamily receptor kinases.

Supplemental Figure S4. Temperature-sensitive root hair growth in *fer-ts/fer-4* and *fer-ts/fer-5* F1 plants.

Supplemental Figure S5. In elevated temperatures, the *fer-ts* mutant responds to hormone treatments similarly to *fer-4* and *fer-5* mutants.

Supplemental Figure S6. Hormonal effects on primary root length, total lateral root number, fresh weight and total leaf number in normal and elevated temperature conditions for *fer-ts*, *fer-4*, and *fer-5* plants.

Supplemental Movie S1. Time-lapse imaging of growing root hair of WT and *fer-ts* mutants during permissive and non-permissive temperatures.

Supplemental Movie S2. Dynamics of YFP fused FERONIA protein localization in growing root hair.

Supplemental Movie S3. FER(WT)-EYFP and FER(G41S)-EYFP protein localization in root hairs at normal (20°C) and elevated (30°C) temperature conditions.

Supplemental Movie S4. Effect of RALF1 peptide on root hair growth.

Supplemental Table S1. List of primers used in this study.

Acknowledgments

We thank to Dr Hen-Ming Wu and Dr Alice Cheung (University of Massachusetts) for providing *fer-4* and *fer-5* mutants, and Jiyuan Yang for assistance in assembling and editing the manuscript.

Funding

This research was supported by the U.S. Department of Energy Office of Science, Office of Basic Energy Sciences, Physical Biosciences program (DE-FG02-07ER15887; S.P., F.G., J.C., and E.N,), the National Science Foundation under Grant No. 1817697 (A.A., H.M, and E.N.), and the BK21plus program of the Ministry of Education, Science and Technology in Korea (D.K., S-J.J., and J-D.B.). This work used the Extreme Science and Engineering Discovery Environment (XSEDE; (John W Towns, 2014), which is supported by National Science Foundation grant number ACI-1548562.

Conflict of interest statement. There are no conflicts of interest associated with this publication.

References

Bell CJ, Ecker JR (1994) Assignment of 30 microsatellite loci to the linkage map of Arabidopsis. Genomics **19:** 137–144

Boisson-Dernier A, Roy S, Kritsas K, Grobei MA, Jaciubek M, Schroeder JI, Grossniklaus U (2009) Disruption of the pollen-expressed FERONIA homologs ANXUR1 and ANXUR2 triggers pollen tube discharge. Development **136:** 3279–3288

Carol RJ, Dolan L (2006) The role of reactive oxygen species in cell growth: lessons from root hairs. J Exp Bot **57:** 1829–1834

Chen J, Yu F, Liu Y, Du C, Li X, Zhu S, Wang X, Lan W, Rodriguez PL, Liu X, et al. (2016) FERONIA interacts with ABI2-type phosphatases to facilitate signaling cross-talk between abscisic acid and RALF peptide in Arabidopsis. Proc Natl Acad Sci U S A **113:** E5519–E5527

Cheung AY, Wu HM (2011) THESEUS 1, FERONIA and relatives: a family of cell wall-sensing receptor kinases? Curr Opin Plant Biol **14:** 632–641

Cho HT, Cosgrove DJ (2002) Regulation of root hair initiation and expansin gene expression in Arabidopsis. Plant Cell **14:** 3237–3253

Clough SJ, Bent AF (1998) Floral dip: a simplified method for Agrobacterium-mediated transformation of Arabidopsis thaliana. Plant J **16:** 735–743

Cole RA, Fowler JE (2006) Polarized growth: maintaining focus on the tip. Curr Opin Plant Biol **9:** 579–588

Deslauriers SD, Larsen PB (2010) FERONIA is a key modulator of brassinosteroid and ethylene responsiveness in Arabidopsis hypocotyls. Mol Plant **3:** 626–640

Du S, Qu LJ, Xiao J (2018) Crystal structures of the extracellular domains of the CrRLK1L receptor-like kinases ANXUR1 and ANXUR2. Protein Sci **27:** 886–892

Duan Q, Kita D, Johnson EA, Aggarwal M, Gates L, Wu HM, Cheung AY (2014) Reactive oxygen species mediate pollen tube rupture to release sperm for fertilization in Arabidopsis. Nat Commun **5:** 3129

Duan Q, Kita D, Li C, Cheung AY, Wu HM (2010) FERONIA receptor-like kinase regulates RHO GTPase signaling of root hair development. Proc Natl Acad Sci U S A **107:** 17821–17826

Duan Q, Liu MJ, Kita D, Jordan SS, Yeh FJ, Yvon R, Carpenter H, Federico AN, Garcia-Valencia LE, Eyles SJ, et al. (2020) FERONIA controls pectin- and nitric oxide-mediated male-female interaction. Nature **579:** 561–566

Escobar-Restrepo JM, Huck N, Kessler S, Gagliardini V, Gheyselinck J, Yang WC, Grossniklaus U (2007) The FERONIA receptor-like kinase mediates male-female interactions during pollen tube reception. Science **317:** 656–660

Feng W, Kita D, Peaucelle A, Cartwright HN, Doan V, Duan Q, Liu MC, Maman J, Steinhorst L, Schmitz-Thom I, et al. (2018) The FERONIA receptor kinase maintains cell-wall integrity during salt stress through Ca(2 +) signaling. Curr Biol **28:** 666–675. e665

Foreman J, Demidchik V, Bothwell JHF, Mylona P, Miedema H, Torres MA, Linstead P, Costa S, Brownlee C, Jones JDG, et al. (2003) Reactive oxygen species produced by NADPH oxidase regulate plant cell growth. Nature **422:** 442–446

Ge Z, Bergonci T, Zhao Y, Zou Y, Du S, Liu MC, Luo X, Ruan H, Garcia-Valencia LE, Zhong S, et al. (2017) Arabidopsis pollen tube integrity and sperm release are regulated by RALF-mediated signaling. Science **358:** 1596–1600

Gilroy S, Jones DL (2000) Through form to function: root hair development and nutrient uptake. Trends Plant Sci **5:** 56–60

Gonneau M, Desprez T, Martin M, Doblas VG, Bacete L, Miart F, Sormani R, Hematy K, Renou J, Landrein B, et al. (2018) Receptor kinase THESEUS1 is a rapid alkalinization factor 34 receptor in arabidopsis. Curr Biol **28:** 2452–2458, e2454

Guo H, Li L, Ye H, Yu X, Algreen A, Yin Y (2009) Three related receptor-like kinases are required for optimal cell elongation in Arabidopsis thaliana. Proc Natl Acad Sci U S A **106:** 7648–7653

Haruta M, Sabat G, Stecker K, Minkoff BB, Sussman MR (2014) A peptide hormone and its receptor protein kinase regulate plant cell expansion. Science **343:** 408–411

Hematy K, Hofte H (2008) Novel receptor kinases involved in growth regulation. Curr Opin Plant Biol **11:** 321–328

Hematy K, Sado PE, Van Tuinen A, Rochange S, Desnos T, Balzergue S, Pelletier S, Renou JP, Hofte H (2007) A receptor-like kinase mediates the response of Arabidopsis cells to the inhibition of cellulose synthesis. Curr Biol **17:** 922–931

Hepler PK, Vidali L, Cheung AY (2001) Polarized cell growth in higher plants. Annu Rev Cell Dev Biol **17:** 159–187

Huang GQ, Li E, Ge FR, Li S, Wang Q, Zhang CQ, Zhang Y (2013) Arabidopsis RopGEF4 and RopGEF10 are important for FERONIA-mediated developmental but not environmental regulation of root hair growth. New Phytol **200:** 1089–1101

Huck N, Moore JM, Federer M, Grossniklaus U (2003) The Arabidopsis mutant feronia disrupts the female gametophytic control of pollen tube reception. Development **130:** 2149–2159

John Towns, Timothy Cockerill, Maytal Dahan, Ian Foster, Kelly Gaither, Andrew Grimshaw, Victor Hazlewood, Scott Lathrop, Dave Lifka, Gregory D. Peterson, et al. (2014) XSEDE: Accelerating scientific discovery. Comput Sci Eng **16:** 62–74

Jones MA, Shen JJ, Fu Y, Li H, Yang Z, Grierson CS (2002) The Arabidopsis Rop2 GTPase is a positive regulator of both root hair initiation and tip growth. Plant Cell **14:** 763–776

Lehti-Shiu MD, Zou C, Hanada K, Shiu SH (2009) Evolutionary history and stress regulation of plant receptor-like kinase/pelle genes. Plant Physiol **150:** 12–26

Li C, Wu HM, Cheung AY (2016) FERONIA and her pals: functions and mechanisms. Plant Physiol **171:** 2379–2392

Lindner H, Muller LM, Boisson-Dernier A, Grossniklaus U (2012) CrRLK1L receptor-like kinases: not just another brick in the wall. Curr Opin Plant Biol **15:** 659–669

Liu X, Castro CA, Wang Y, Noble JA, Ponvert ND, Bundy MG, Hoel CR, Shpak ED, Palanivelu R (2016) The Role of LORELEI in Pollen Tube Reception at the Interface of the Synergid Cell and Pollen Tube Requires the Modified Eight-Cysteine Motif and the Receptor-Like Kinase FERONIA. Plant Cell **28**: 1035–52.

Miyazaki S, Murata T, Sakurai-Ozato N, Kubo M, Demura T, Fukuda H, Hasebe M (2009) ANXUR1 and 2, sister genes to FERONIA/SIRENE, are male factors for coordinated fertilization. Curr Biol **19:** 1327–1331

Molendijk AJ, Bischoff F, Rajendrakumar CS, Friml J, Braun M, Gilroy S, Palme K (2001) Arabidopsis thaliana Rop GTPases are localized to tips of root hairs and control polar growth. EMBO J **20:** 2779–2788

Morillo SA, Tax FE (2006) Functional analysis of receptor-like kinases in monocots and dicots. Curr Opin Plant Biol **9:** 460–469

Muller LN, Muhle-Goll C, Biskup MB (2010) The Glc2Man2-fragment of the N-glycan precursor–a novel ligand for the glycan-binding protein malectin? Org Biomol Chem **8:** 3294–3299

Ngo QA, Vogler H, Lituiev DS, Nestorova A, Grossniklaus U (2014) A calcium dialog mediated by the FERONIA signal transduction pathway controls plant sperm delivery. Dev Cell **29:** 491–500

Pearce G, Moura DS, Stratmann J, Ryan CA Jr. (2001) RALF, a 5-kDa ubiquitous polypeptide in plants, arrests root growth and development. Proc Natl Acad Sci U S A **98:** 12843–12847

Preuss ML, Santos-Serna J, Falbel TG, Bednarek SY, Nielsen E (2004) The Arabidopsis Rab GTPase RabA4b localizes to the tips of growing root hair cells. Plant Cell **16:** 1589–1603

Preuss ML, Schmitz AJ, Thole JM, Bonner HK, Otegui MS, Nielsen E (2006) A role for the RabA4b effector protein PI-4Kbeta1 in polarized expansion of root hair cells in Arabidopsis thaliana. J Cell Biol **172:** 991–998

Rotman N, Rozier F, Boavida L, Dumas C, Berger F, Faure JE (2003) Female control of male gamete delivery during fertilization in Arabidopsis thaliana. Curr Biol **13:** 432–436

Schallus T, Jaeckh C, Feher K, Palma AS, Liu Y, Simpson JC, Mackeen M, Stier G, Gibson TJ, Feizi T, et al. (2008) Malectin: a novel carbohydrate-binding protein of the endoplasmic reticulum and a candidate player in the early steps of protein N-glycosylation. Mol Biol Cell **19:** 3404–3414

Schindelin J, Arganda-Carreras I, Frise E, Kaynig V, Longair M, Pietzsch T, Preibisch S, Rueden C, Saalfeld S, Schmid B, et al. (2012) Fiji: an open-source platform for biological-image analysis. Nat Methods **9:** 676–682

Schoenaers S, Balcerowicz D, Breen G, Hill K, Zdanio M, Mouille G, Holman TJ, Oh J, Wilson MH, Nikonorova N, et al. (2018) The auxin-regulated CrRLK1L kinase ERULUS controls cell wall composition during root hair tip growth. Curr Biol **28:** 722–732, e726

Schulze-Muth P, Irmler S, Schroder G, Schroder J (1996) Novel type of receptor-like protein kinase from a higher plant (Catharanthus roseus). cDNA, gene, intramolecular autophosphorylation, and identification of a threonine important for auto- and substrate phosphorylation. J Biol Chem **271:** 26684–26689

Shih HW, Miller ND, Dai C, Spalding EP, Monshausen GB (2014) The receptor-like kinase FERONIA is required for mechanical signal transduction in Arabidopsis seedlings. Curr Biol **24:** 1887–1892

Shiu SH, Bleecker AB (2001) Plant receptor-like kinase gene family: diversity, function, and signaling. Sci STKE **2001:** re22

Shiu SH, Bleecker AB (2003) Expansion of the receptor-like kinase/Pelle gene family and receptor-like proteins in Arabidopsis. Plant Physiol **132:** 530–543

Smith IF, Hitt B, Green KN, Oddo S, LaFerla FM (2005) Enhanced caffeine-induced Ca2 + release in the 3xTg-AD mouse model of Alzheimer's disease. J Neurochem **94:** 1711–1718

Stegmann M, Monaghan J, Smakowska-Luzan E, Rovenich H, Lehner A, Holton N, Belkhadir Y, Zipfel C (2017) The receptor kinase FER is a RALF-regulated scaffold controlling plant immune signaling. Science **355:** 287–289

Thole JM, Vermeer JE, Zhang Y, Gadella TW Jr, Nielsen E (2008) Root hair defective4 encodes a phosphatidylinositol-4-phosphate phosphatase required for proper root hair development in Arabidopsis thaliana. Plant Cell **20:** 381–395

Weigel D, Glazebrook J (2006) EMS mutagenesis of Arabidopsis seed. CSH Protoc **2006**: 1256–1260

Xiao Y, Stegmann M, Han Z, DeFalco TA, Parys K, Xu L, Belkhadir Y, Zipfel C, Chai J (2019) Mechanisms of RALF peptide perception by a heterotypic receptor complex. Nature **572:** 270–274

Yang J, Bak G, Burgin T, Mayes HB, Pena MJ, Urbanowicz B, Barnes WJ, Nielsen E (2020) Biochemical and genetic analysis identify CSLD3 as a beta-1,4-glucan synthase that functions during plant cell wall synthesis. Plant Cell **32:** 1749–1767

Yu F, Li J, Huang Y, Liu L, Li D, Chen L, Luan S (2014) FERONIA receptor kinase controls seed size in Arabidopsis thaliana. Mol Plant **7:** 920–922

Yu F, Qian L, Nibau C, Duan Q, Kita D, Levasseur K, Li X, Lu C, Li H, Hou C, et al. (2012) FERONIA receptor kinase pathway suppresses abscisic acid signaling in Arabidopsis by activating ABI2 phosphatase. Proc Natl Acad Sci U S A **109:** 14693–14698